



BNXXXX-v0.0  
October 8, 2025

# Measurement of inclusive $B \rightarrow \Lambda_c$ branching fractions using Belle data and hadronic Full Event Interpretation

Leonardo Benjamin Rizzato<sup>1</sup>.

<sup>1</sup>*Institute Jožef Stefan, Ljubljana, Slovenia*

## **Abstract**

Inclusive  $B \rightarrow \Lambda_c$  branching fractions were measured most recently by BaBar collaboration. However, the measurement still presented a poor accuracy. A more precise measurement of inclusive  $B \rightarrow \Lambda_c$  branching fraction could be useful to gain a better confidence on B meson weak decays treatment. With help of the Full Event Interpretation algorihm, it is possible to perform a more precise measurement of inclusive  $B \rightarrow \Lambda_c$  branching fractions using Belle data set.





# Contents

<b>1</b>	<b>Introduction</b>	<b>1</b>
1.1	Analysis Setup . . . . .	1
1.2	Datasets . . . . .	1
<b>2</b>	<b>Event selection and reconstruction</b>	<b>3</b>
2.1	$B_{tag}$ reconstruction . . . . .	3
2.2	$\Lambda_c$ reconstruction . . . . .	3
2.3	Wrongly reconstructed $B_{tag}$ candidates . . . . .	4
2.4	Signal selection optimization . . . . .	6
2.4.1	$B^- \rightarrow \Lambda_c^+$ decays . . . . .	7
2.4.2	$B^+ \rightarrow \Lambda_c^+$ decays . . . . .	10
2.4.3	$\bar{B}^0 \rightarrow \Lambda_c^+$ decays . . . . .	14
2.4.4	$B^0 \rightarrow \Lambda_c^+$ decays . . . . .	18
<b>3</b>	<b>2D simultaneous fit</b>	<b>21</b>
3.1	Probability Density Functions (PDFs) for the two dimensional fit . . . . .	21
3.1.1	Total Signal fits . . . . .	21
3.1.2	Mbc peaking and flat background . . . . .	23
3.1.3	Crossfeed background . . . . .	25
3.1.4	Continuum background . . . . .	27
3.2	Two dimensional fit on Monte Carlo . . . . .	35
3.2.1	Fit results for $B^- \rightarrow \Lambda_c^+$ decays . . . . .	37
3.2.2	Fit results for $B^- \rightarrow \bar{\Lambda}_c^-$ decays . . . . .	39
3.2.3	Fit results for $\bar{B}^0 \rightarrow \Lambda_c^+$ decays . . . . .	41
3.2.4	Fit results for $\bar{B}^0 \rightarrow \bar{\Lambda}_c^-$ decays . . . . .	43
3.2.5	Fit residuals . . . . .	44
3.2.6	toy Monte Carlo study . . . . .	46
<b>4</b>	<b><math>B_{tag}</math> fit</b>	<b>48</b>
4.1	Probability Density Functions (PDFs) for the $B_{tag}$ . . . . .	48
4.1.1	Total Signal fits . . . . .	48
4.1.2	Crossfeed PDF . . . . .	50
4.1.3	Continuum PDF . . . . .	53

4.2	$B_{tag}$ fit . . . . .	54
4.2.1	Fit results for $B^- \rightarrow \Lambda_c^+$ decays . . . . .	54
4.2.2	Fit results for $B^- \rightarrow \bar{\Lambda}_c^-$ decays . . . . .	55
4.2.3	Fit results for $\bar{B}^0 \rightarrow \Lambda_c^+$ decays . . . . .	56
4.2.4	Fit results for $\bar{B}^0 \rightarrow \bar{\Lambda}_c^+$ decays . . . . .	57
<b>5</b>	<b>Efficiencies</b>	<b>59</b>
5.1	FEI Efficiencies . . . . .	59
5.1.1	Generic FEI efficiency . . . . .	59
5.1.2	Signalside-dependent FEI efficiency . . . . .	60
5.2	$\Lambda_c$ efficiency . . . . .	61
5.2.1	$B^- \rightarrow \Lambda_c^+$ decays . . . . .	61
5.2.2	$B^- \rightarrow \bar{\Lambda}_c^-$ decays . . . . .	61
5.2.3	$\bar{B}^0 \rightarrow \Lambda_c^+$ decays . . . . .	61
5.2.4	$\bar{B}^0 \rightarrow \bar{\Lambda}_c^-$ decays . . . . .	61
<b>6</b>	<b>Branching ratio</b>	<b>62</b>
6.1	Systematics . . . . .	63
6.1.1	Continuum background . . . . .	63
6.1.2	Crossfeed ratio . . . . .	66
6.1.3	Crossfeed $B_{tag}$ PDF . . . . .	66
6.1.4	2DFit crossfeed normalization . . . . .	66
6.1.5	2DFit $M_{bc}$ peaking/flat PDFs . . . . .	67
6.1.6	PID efficiency correction . . . . .	67
6.1.7	$B^- \rightarrow \Lambda_c^+$ decays . . . . .	68
6.1.8	$B^+ \rightarrow \Lambda_c^+$ decays . . . . .	69
References . . . . .		70

# <sup>1</sup> Chapter 1

## <sup>2</sup> Introduction

<sup>3</sup> Inclusive  $B$  meson baryonic decays with a  $\Lambda_c$  baryon in the final state are the most  
<sup>4</sup> abundant, due to a relatively large  $V_{cb}$  element of the CKM matrix. The *BaBar* experiment  
<sup>5</sup> measured their branching fractions to be around the percent level (see ref. [1]). However, the  
<sup>6</sup> branching fractions were determined with big uncertainties: nearly 50% on the measured  
<sup>7</sup> values or, in the case of the  $B^0 \rightarrow \Lambda_c^+$  decay, only an upper limit could be established.  
<sup>8</sup> A more precise measurement of inclusive  $B \rightarrow \Lambda_c$  branching fractions may shed light on  
<sup>9</sup> the appropriateness of  $B$  meson weak decays treatment, particularly of strong interaction  
<sup>10</sup> effects modelling. Predictions for inclusive branching fractions are given, for example, in  
<sup>11</sup> ref. [2] or in [3] for  $B \rightarrow \Lambda_c p$  decays.

<sup>12</sup> Exploiting the Full Event Interpretation (FEI) algorithm, developed for the Belle  
<sup>13</sup> II experiment, it may be possible to perform a more precise measurement of inclusive  
<sup>14</sup>  $B \rightarrow \Lambda_c$  branching fractions, using the full Belle data set. A more precise measurement  
<sup>15</sup> may also trigger further research on currently scarce theory predictions for  $B$  meson decays  
<sup>16</sup> to charm baryons.

### <sup>17</sup> 1.1 Analysis Setup

<sup>18</sup> The reconstruction is performed with **BASF2** release 05-02-03 together with the **b2bii**  
<sup>19</sup> package in order to convert the *Belle* MDST files (**BASF** data format) to *Belle II* MDST files  
<sup>20</sup> (**BASF2** data format). The FEI version used is **FEI\_B2BII\_light-2012-minos**.

### <sup>21</sup> 1.2 Datasets

<sup>22</sup> The Belle detector acquired a dataset of about  $L_0 \approx 710 fb^{-1}$  of integrated luminosity in  
<sup>23</sup> its lifetime at the  $\Upsilon(4S)$  energy of 10.58 GeV, which corresponds to about  $771 \times 10^6 B\bar{B}$   
<sup>24</sup> meson pairs. Additionally, several streams of Monte-Carlo (MC) samples were produced,  
<sup>25</sup> where each stream of MC corresponds to the same amount of data that was taken with  
<sup>26</sup> the detector. No specific signal MC was used: instead of producing dedicated signal MC

<sup>27</sup> samples, the samples were obtained by filtering the decays of interest from the generic  
<sup>28</sup> on-resonance MC samples. The following samples were used in this analysis:

- <sup>29</sup>     • data
- <sup>30</sup>     • MC - 6 streams of  $B^+B^-$  and  $B^0\bar{B}^0$  (denoted as `charged` and `mixed`) for signal  
<sup>31</sup>       decays and backgrounds (if more of the in total existing 10 streams is used it is  
<sup>32</sup>       explicitly specified throughout this note).
  - <sup>33</sup>       - 6 streams of  $q\bar{q}$  produced at  $\Upsilon(4S)$  resonance energy
  - <sup>34</sup>       - 6 streams of  $q\bar{q}$  produced at 60 MeV below  $\Upsilon(4S)$  resonance energy, where each  
<sup>35</sup>       stream corresponds to  $1/10 \times L_0$ .

<sup>36</sup>

<sup>37</sup> **Chapter 2**

<sup>38</sup> **Event selection and reconstruction**

<sup>39</sup> In this chapter the procedure for reconstruction of the events where one  $B$  meson decays  
<sup>40</sup> inclusively to a  $\Lambda_c$  baryon and the accompanying  $B$  meson decays hadronically is illustrated.

<sup>41</sup> **2.1  $B_{tag}$  reconstruction**

<sup>42</sup> The FEI is an exclusive tagging algorithm that uses machine learning to reconstruct  
<sup>43</sup>  $B$  meson decay chains and calculates the probability that these decay chains correctly  
<sup>44</sup> describe the true process. In this analysis only hadronically reconstructed decay chains  
<sup>45</sup> are considered. The training called `FEI_B2BII_light-2012-minos` is used. Tag-side  $B$   
<sup>46</sup> meson candidates are required to have a beam-constrained mass greater than  $5.22 \text{ GeV}/c^2$   
<sup>47</sup> and  $-0.15 < \Delta E < 0.07 \text{ GeV}$ .

<sup>48</sup> In the case of multiple candidates in the same event, the candidate with the highest  
<sup>49</sup> SignalProbability (the signal probability calculated by FEI using FastBDT) is chosen. To  
<sup>50</sup> suppress the background consisting of  $B^0$  events misreconstructed as  $B^+$  (and vice-versa)  
<sup>51</sup> from neutral (charged) decays also a  $B^0$  ( $B^+$ ) candidate is reconstructed with FEI and if  
<sup>52</sup> its SignalProbability is higher than the charged (neutral) reconstructed  $B$  meson, the event  
<sup>53</sup> is discarded. This constitutes a sort of crossfeed-veto, rejecting part of events belonging  
<sup>54</sup> to the other typology of decays of interest: for example in the case one is interested  
<sup>55</sup> in reconstructing  $B^{+/-}$  decays and the event actually contains  $B^0/\bar{B}^0$  decays, the FEI  
<sup>56</sup> reconstructed neutral  $B$  meson candidate most likely presents a higher SignalProbability  
<sup>57</sup> than the charged FEI reconstructed candidate.

<sup>58</sup> **2.2  $\Lambda_c$  reconstruction**

<sup>59</sup> In the *rest of event* (ROE) of the reconstructed  $B_{tag}$  meson, to select  $\Lambda_c \rightarrow pK\pi$  signal  
<sup>60</sup> candidates, the following event selection criteria are applied (same PID cuts were used for  
<sup>61</sup> example in the Belle Note 1521 [https://belle.kek.jp/secured/belle\\_note/gn1521/BN\\_v1.pdf](https://belle.kek.jp/secured/belle_note/gn1521/BN_v1.pdf)). Charged tracks with the impact parameters perpendicular to and along the  
<sup>62</sup> nominal interaction point (IP) are required to be less than 2 cm and 4 cm respectively  
<sup>63</sup>

64 ( $dr < 2$  cm and  $|dz| < 4$  cm).  
 65 The pion tracks are required to be identified with  $\frac{\mathcal{L}_\pi}{\mathcal{L}_K + \mathcal{L}_\pi} > 0.6$ . The kaon tracks are  
 66 required to be identified with  $\frac{\mathcal{L}_K}{\mathcal{L}_K + \mathcal{L}_\pi} > 0.6$ , and the proton/anti-proton tracks are  
 67 required to be identified with  $\frac{\mathcal{L}_{p/\bar{p}}}{\mathcal{L}_K + \mathcal{L}_{p/\bar{p}}} > 0.6$  and  $\frac{\mathcal{L}_{p/\bar{p}}}{\mathcal{L}_\pi + \mathcal{L}_{p/\bar{p}}} > 0.6$ , where the  $\mathcal{L}_{\pi,K,p/\bar{p}}$  are the  
 68 likelihoods for pion, kaon, proton/anti-proton, respectively, determined using the ratio of  
 69 the energy deposit in the ECL to the momentum measured in the SVD and CDC, the  
 70 shower shape in the ECL, the matching between the position of charged track trajectory  
 71 and the cluster position in the ECL, the hit information from the ACC and the dE/dx  
 72 information in the CDC.  
 73 For the  $\Lambda_c$  candidates a vertex fit is performed with **TreeFitter**, requiring it to converge.  
 74 If there are more than one  $\Lambda_c$  combination, then the best candidate based on the  $\chi^2$   
 75 probability is chosen. The  $\Lambda_c$  signal region is defined to be  $|M_{\Lambda_c} - m_{\Lambda_c}| < 20$  MeV/ $c^2$  ( $\sim$   
 76  $3\sigma$ ), here  $m_{\Lambda_c}$  is the nominal mass of  $m_{\Lambda_c}$ .

77

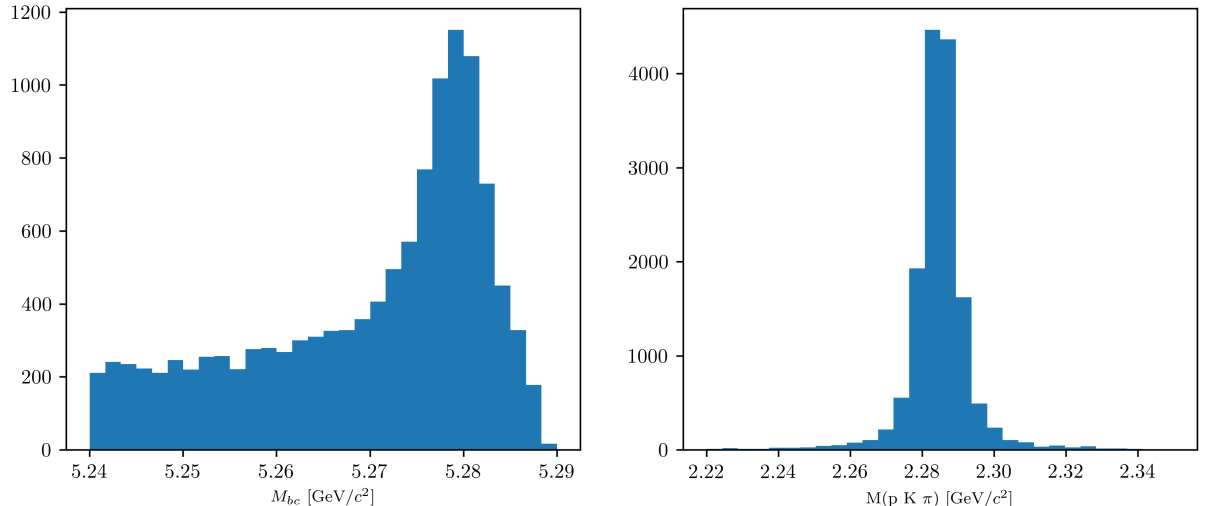


Figure (2.1)  $M_{bc}$  and  $M(pK\pi)$  distributions of  $B_{tag}$  and  $\Lambda_c$  candidates reconstructed in the signal sample.

## 78 2.3 Wrongly reconstructed $B_{tag}$ candidates

79 In the case of the signal sample the distributions for the beam-constrained mass  $M_{bc}$  and  
 80 for the correctly reconstructed  $\Lambda_c$  candidates, look like in Fig. 2.1. If one then investigates  
 81 the  $M_{bc}$  distribution of the  $B_{tag}$  candidates reconstructed with FEI, it can be seen that  
 82 there is a peaking structure for wrongly reconstructed  $B$  mesons (as in Fig. 2.2), according  
 83 to the BASF2 internal truth matching variable **isSignal**. It is obvious from this that the  
 84 BASF2 internal truth matching variable cannot be used to separate properly the signal  
 85 events in correctly and wrongly reconstructed  $B$  mesons. In the study BELLE2-NOTE-TE-

86 2021-026 <https://docs.belle2.org/record/2711/files/BELLE2-NOTE-TE-2021-026.pdf>  
87 a possible solution was found developing new variables that can be used for an  
88 improved truth matching for the FEI (those variables were added to a newer BASF2  
89 release than the one used for this study). In the present study instead a more "traditional"  
90 approach was adopted: fitting the  $M_{bc}$  distribution with a sum of PDFs that account for the  
91 flat (background) component and the peaking (signal) component. The first component  
92 represents the combinatorial background, i.e.  $B$  mesons that were mis-reconstructed,  
93 and therefore those events are denoted from now on as "**misreconstructed signal**".  
94 The peaking component represents the correctly reconstructed signal events in  $M_{bc}$  and  
95 therefore denoted from now on as "**reconstructed signal**". Only the second one is then  
96 considered for the signal yield, while the first is counted as a background. To validate this  
97 method a control decay study was performed on the flavor correlated  $B^+ \rightarrow \bar{D}^0$  channel.

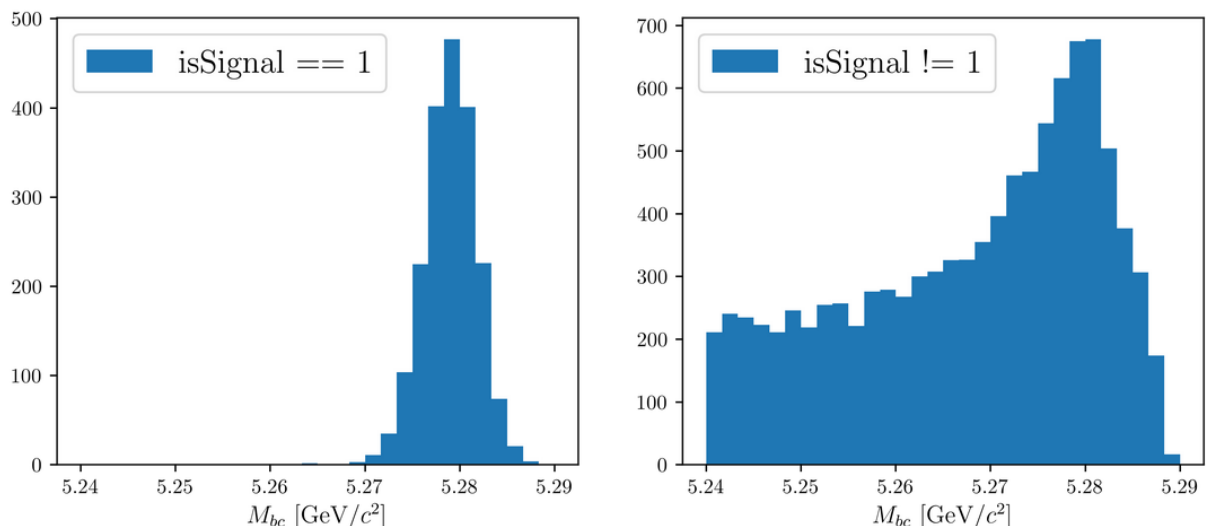


Figure (2.2)  $M_{bc}$  distribution of  $B_{tag}$  candidates reconstructed in the signal sample, truth-matched (on the left) and not (on the right).

## 98 2.4 Signal selection optimization

99 To further enhance the purity of the signal decays, an optimization procedure is adopted  
100 to determine optimal cuts for a set of variables for each decay mode under investigation  
101 by this study. The cuts on the following variables are optimized:

- 102 • *foxWolframR2*: the event based ratio of the 2-nd to the 0-th order Fox-Wolfram  
103 moments
- 104 • SignalProbability: the already mentioned signal probability calculated by FEI using  
105 FastBDT
- 106 •  $p_{CMS}^{\Lambda_c}$ : momentum of the  $\Lambda_c$  candidates in the center of mass system

107 The optimization is based on the Figure Of Merit (FOM):  $FOM = \frac{S}{\sqrt{S+B}}$   
108 Where S and B are respectively signal and background events in the signal region:

109  $M_{bc} > 5.27 \text{ GeV}/c^2$ ,  $2.2665 < M(pK\pi) < 2.3065 \text{ GeV}/c^2$ .

110 Due to the issue reported in Sec. 2.3, to separate signal events that peak in  $M_{bc}$  from  
111 the ones that are not (which are then categorized as background events), the events  
112 reconstructed in the signal sample are fitted with a sum of Crystal Ball function and  
113 Argus for each cut value on the corresponding variable to optimize (as in Fig. 2.3).

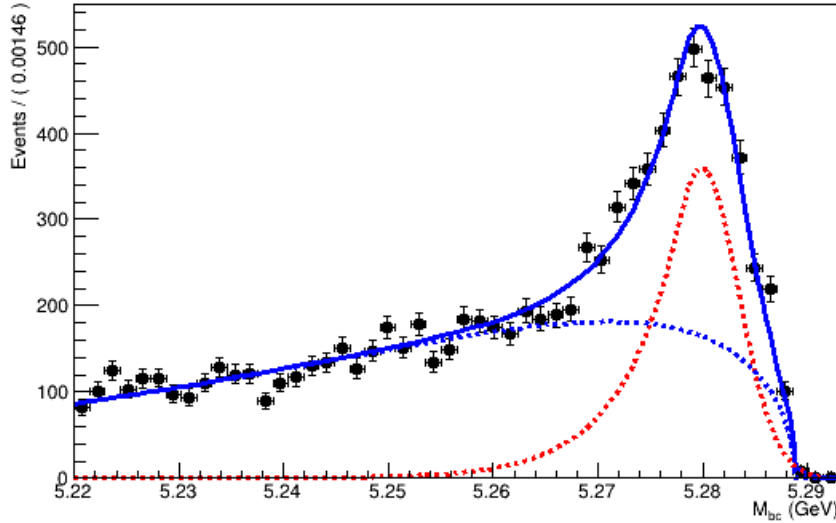


Figure (2.3) Example of a fit used to separate the correctly reconstructed  $B$  mesons (described by the red dotted Crystal Ball function) from the wrongly reconstructed ones (described by the blue dotted Argus function).

114 The next sections illustrate the procedure for each of the four decay channels.

115 **2.4.1  $B^- \rightarrow \Lambda_c^+$  decays**

116 Here below the procedure of optimized signal selection of charged correlated decays is  
117 presented.

118 First, in order to suppress the continuum background the cut on *foxWolframR2* is  
119 optimized. Fig. 2.4 shows the *foxWolframR2* distributions for signal and continuum  
120 events.

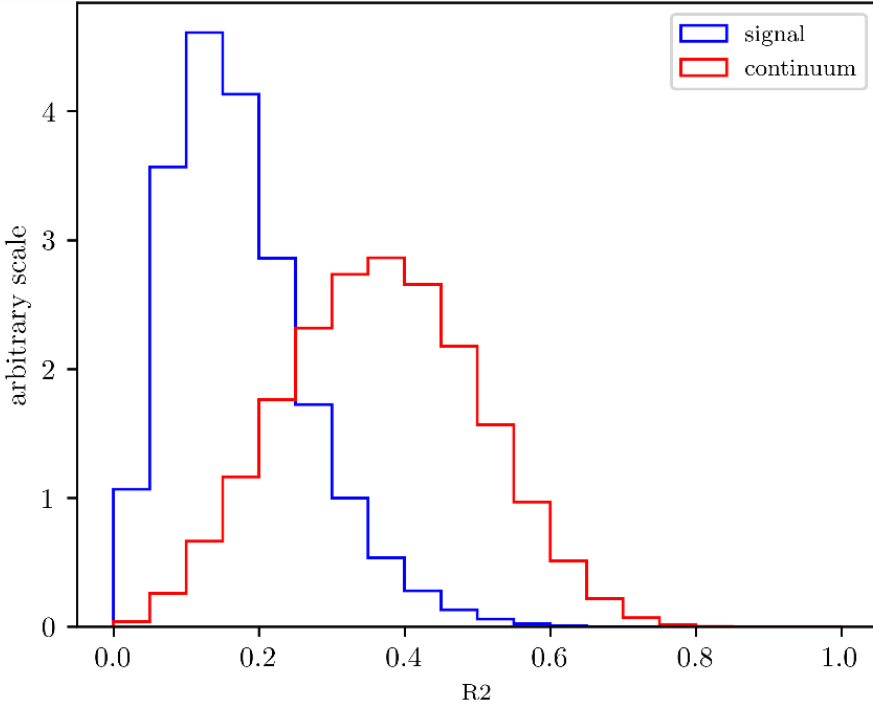


Figure (2.4) Distribution of the *foxWolframR2* variable for signal and continuum background events.

121 With the optimized cut  $\text{foxWolframR2} < 0.27$  (corresponding to the maximum of  
122 the FOM curve shown in Fig. 2.5), the cut on SignalProbability is optimized in the same  
123 way (see Fig. 2.6).

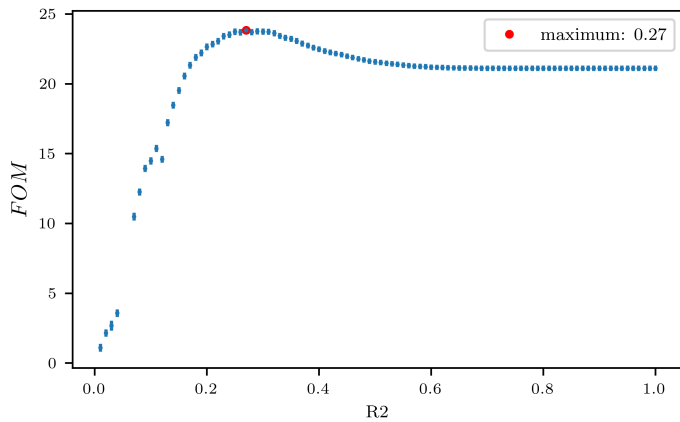


Figure (2.5) Figure of Merit values calculated at several cuts on the *foxWolframR2* variable

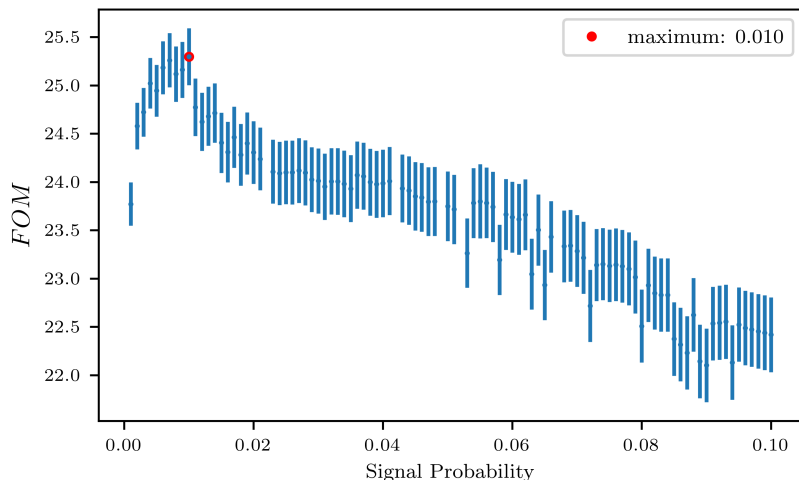


Figure (2.6) Figure of Merit values calculated at several cuts on the *SignalProbability* variable

124      With the optimized cut *SignalProbability* > 0.01, the cut on *foxWolframR2* variable is  
 125      rechecked (Fig. 2.7). Being the maximum values fluctuating around *foxWolframR2* < 0.3,  
 126      this cut is the one finally chosen for this variable.

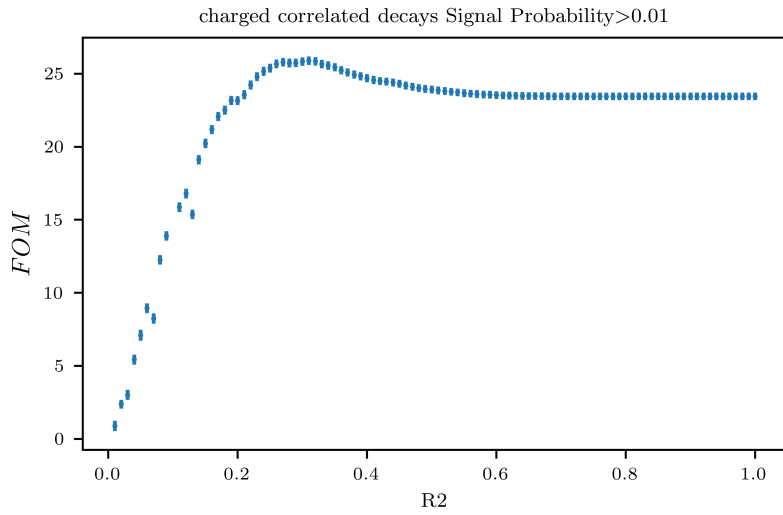


Figure (2.7) Figure of Merit values calculated at several cuts on the *foxWolframR2* variable

127        With the optimized cuts on SignalProbability and *foxWolframR2* variable, the cut  
 128        on  $p_{CMS}^{\Lambda_c}$  is optimized

129

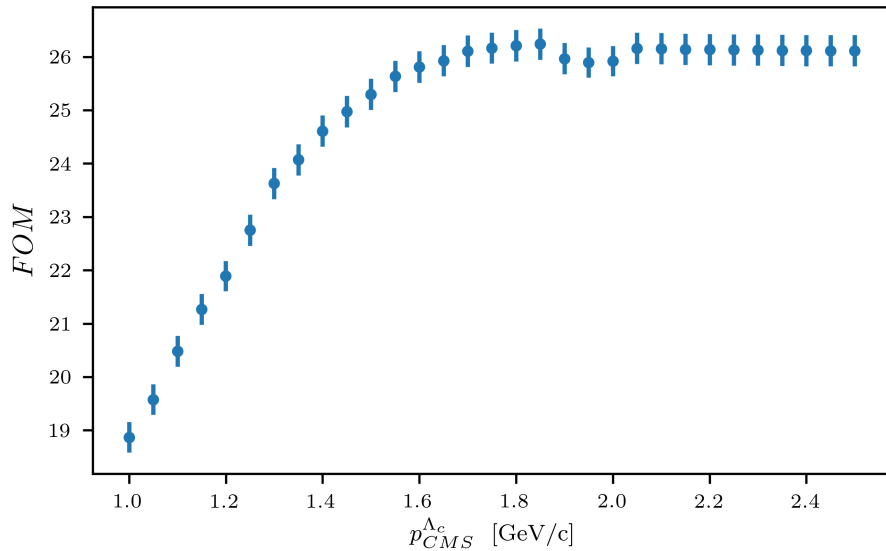


Figure (2.8) Figure of Merit values calculated at several cuts on the momentum of the  $\Lambda_c$  candidates in the center of mass system

130        From Fig. 2.8 one can see that with values of the cut above  $p_{CMS}^{\Lambda_c} < 1.8$   $\text{GeV}/c^2$  a  
 131        plateau of maximum FOM values is reached. But such a cut would still be useful to reject

<sup>132</sup> some background events as one can see from Fig. 2.9.

<sup>133</sup> Finally the optimized selection cuts are:

<sup>134</sup> •  $\text{foxWolframR2} < 0.3$

<sup>135</sup> •  $\text{SignalProbability} > 0.01$

<sup>136</sup> •  $p_{CMS}^{\Lambda_c} < 1.8 \text{ GeV}/c$

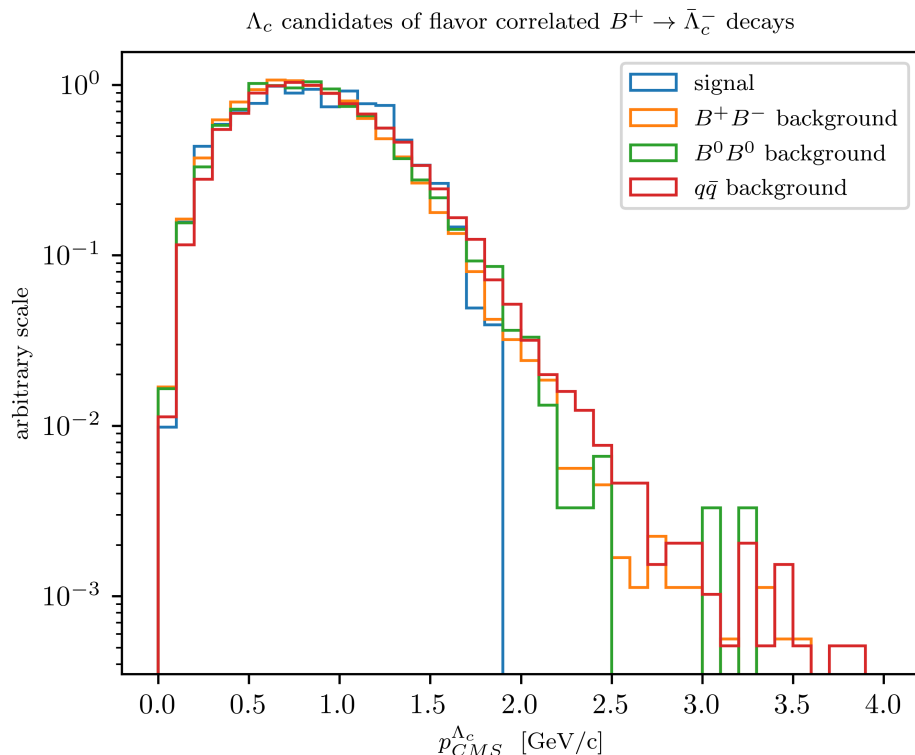


Figure (2.9) Distribution of  $\Lambda_c$  candidates momenta in the center of mass system

#### <sup>137</sup> 2.4.2 $B^+ \rightarrow \Lambda_c^+$ decays

<sup>138</sup> For anticorrelated decays, the same  $\text{foxWolframR2}$  cut is defined after the optimization  
<sup>139</sup> procedure (see Fig. 2.13).

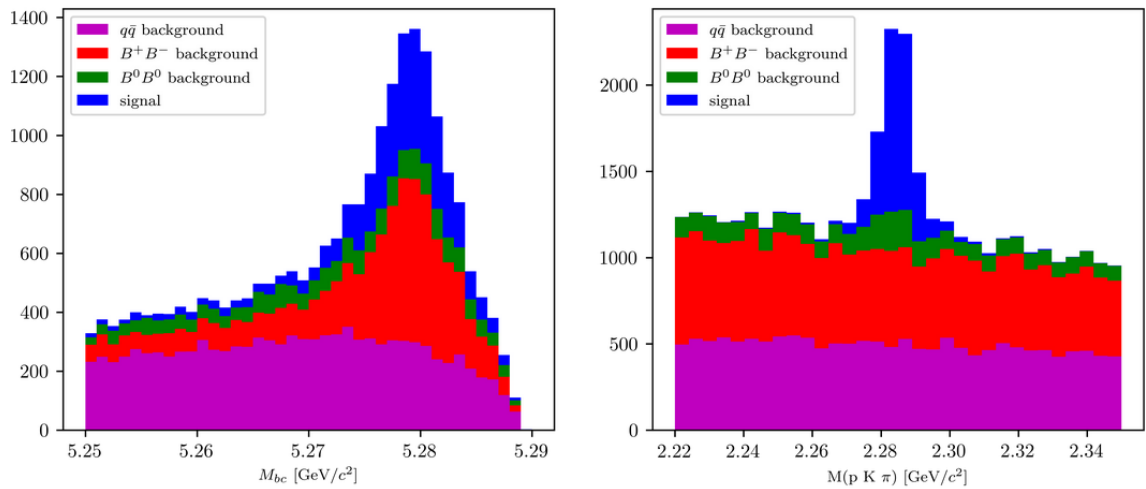


Figure (2.10) Distribution of  $M_{bc}$  (left) and invariant mass of charged correlated  $\Lambda_c$  candidates (right), in the signal region after the above mentioned selection cuts.

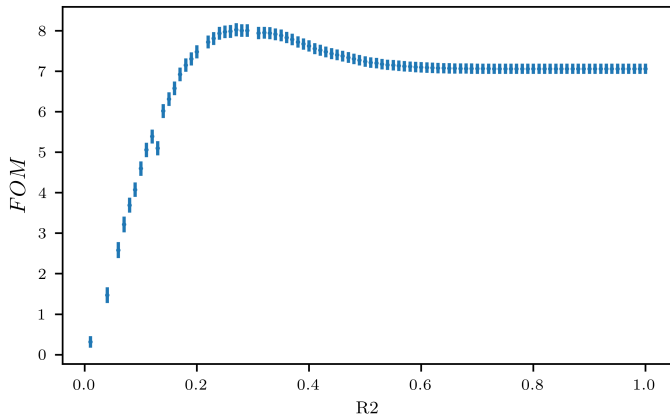


Figure (2.11) Figure of Merit values calculated at several cuts on the  $foxWolframR2$  variable

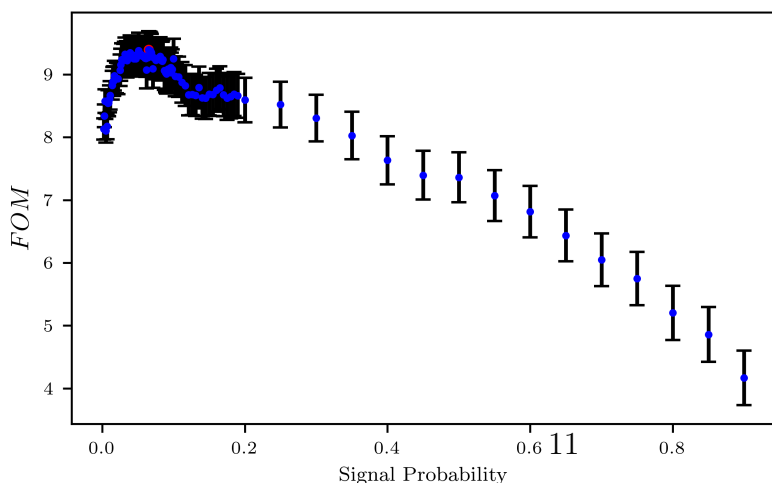


Figure (2.12) Figure of Merit values calculated at several cuts on the SignalProbability variable

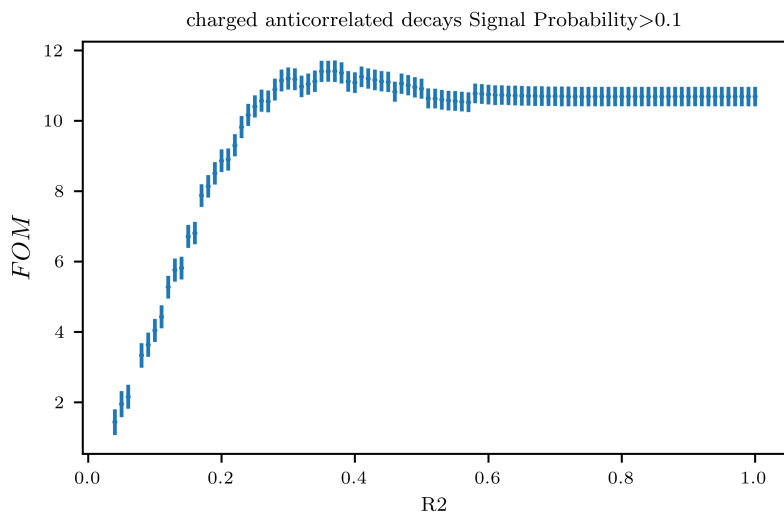


Figure (2.13) Figure of Merit values calculated at several cuts on the *foxWolframR2* variable

<sup>140</sup> With the optimized cuts on SignalProbability and *foxWolframR2* variable, the cut  
<sup>141</sup> on  $p_{CMS}^{\Lambda_c}$  is selected.

<sup>142</sup>

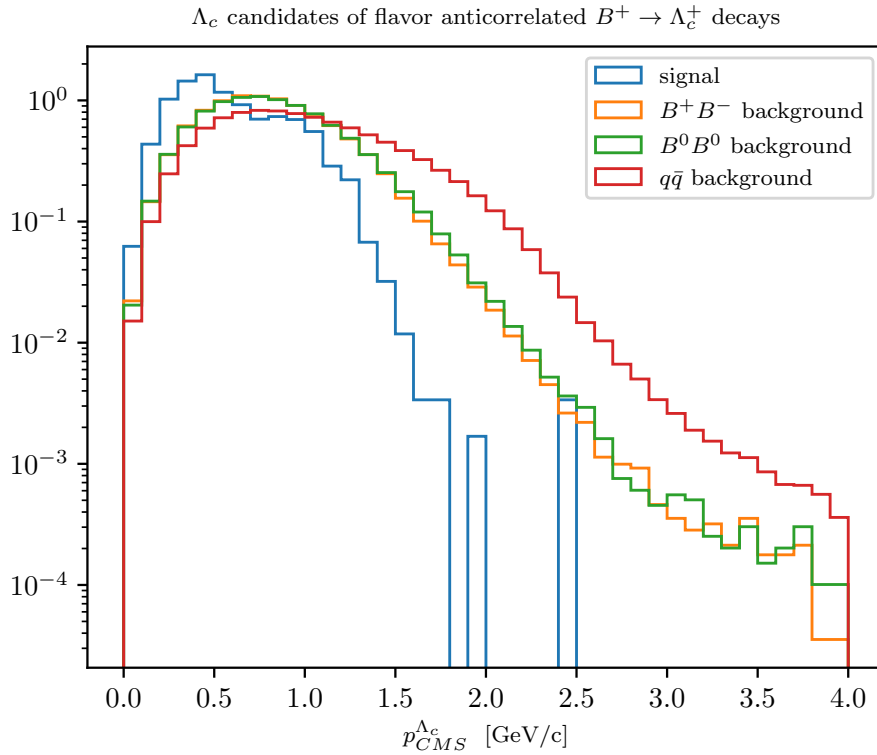


Figure (2.14) Distribution of  $\Lambda_c$  candidates momenta in the center of mass system

<sup>143</sup> The final optimized selection cuts are:

<sup>144</sup> •  $foxWolframR2 < 0.3$

<sup>145</sup> • SignalProbability  $> 0.1$

<sup>146</sup> •  $p_{CMS}^{\Lambda_c} < 1.5$  GeV/c

<sup>147</sup> Fig. 2.15 shows the projections of the  $M_{bc}$  and  $M(pK\pi)$  distributions.

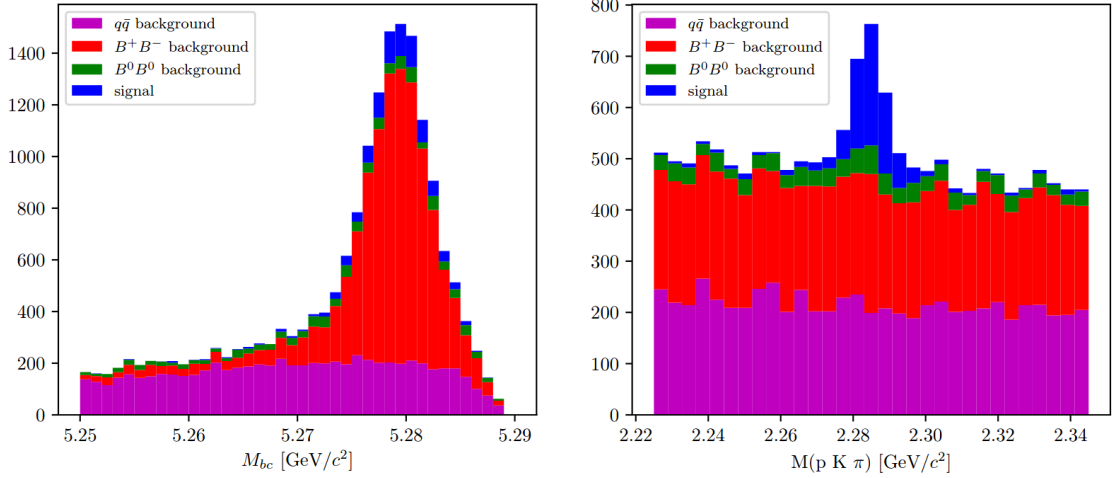


Figure (2.15) Distribution of  $M_{bc}$  (left) and invariant mass of charged correlated  $\Lambda_c$  candidates (right), in the signal region after the above mentioned selection cuts.

#### <sup>148</sup> 2.4.3 $\bar{B}^0 \rightarrow \Lambda_c^+$ decays

<sup>149</sup> Also for neutral correlated decays, first the cut on *foxWolframR2* is optimized.

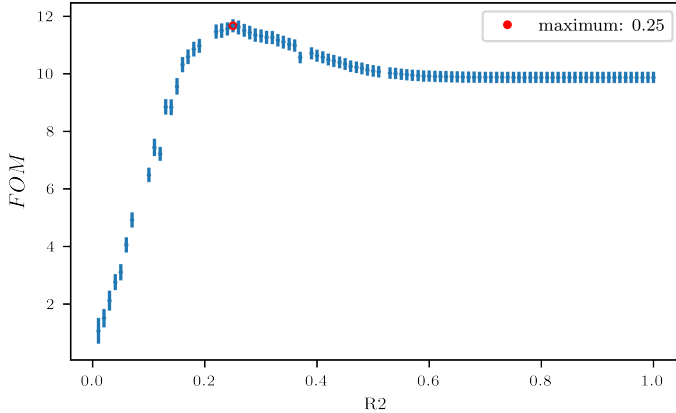


Figure (2.16) Figure of Merit values calculated at several cuts on the *foxWolframR2* variable

<sup>150</sup> The cut suggested by Fig. 2.16,  $foxWolframR2 < 0.27$ , is used to define the cut on <sup>151</sup> the SignalProbability variable. From Fig. 2.17, it seems the optimal cut maximizing the <sup>152</sup> *FOM* would be around 0.05. If one zooms like in Fig. 2.18 one can see that there is a <sup>153</sup> sort of plateau starting around 0.03 and ending after values around 0.11, where the values <sup>154</sup> fluctuate within statistical uncertainties around *FOM* = 13. In this case, a legitimate <sup>155</sup> choice is to use the most stringent cut (*SignalProbability* > 0.11) being the *FOM* same <sup>156</sup> but rejecting more background events.

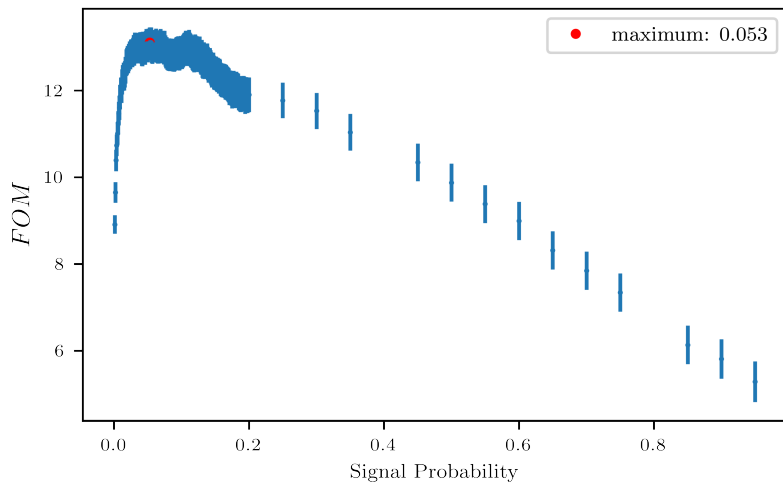


Figure (2.17) Figure of Merit values calculated at several cuts on the SignalProbability variable

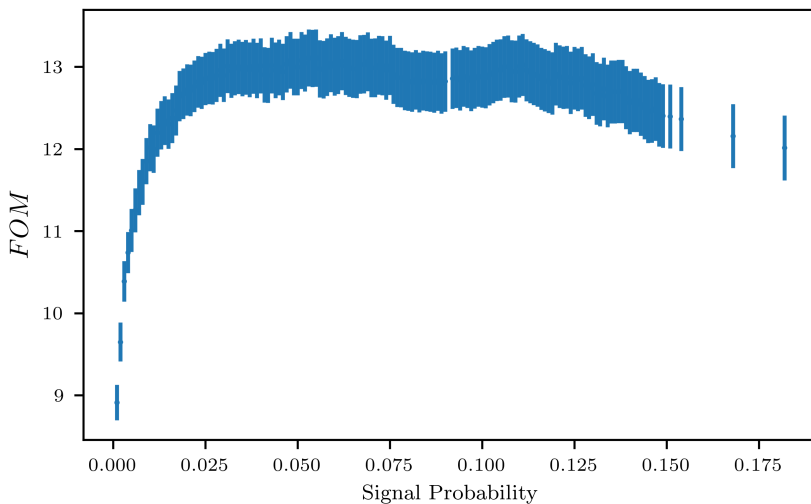


Figure (2.18) Figure of Merit values calculated at several cuts on the SignalProbability variable

157        The *FOM* curve for the *foxWolframR2* variable is rechecked applying the chosen  
 158        cut on *SignalProbability* (Fig. 2.19). As done in the other cases the final cut chosen is  
 159         $\text{foxWolframR2} < 0.3$

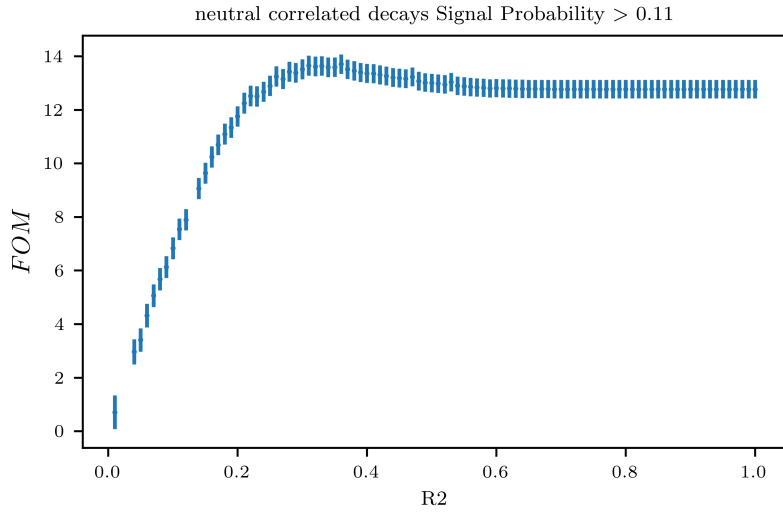


Figure (2.19) Figure of Merit values calculated at several cuts on the *foxWolframR2* variable

160     Using now the two optimized cuts to check the *FOM* curve for the momenta a plateau  
 161   appears for cuts starting from values around  $p_{CMS}^{\Lambda_c} < 1.7 \text{ GeV}/c$  (see Fig. 2.20). In fact,  
 162   around that value the level of background becomes significantly higher compared to the  
 163   amount o signal events as one can see in Fig. 2.21

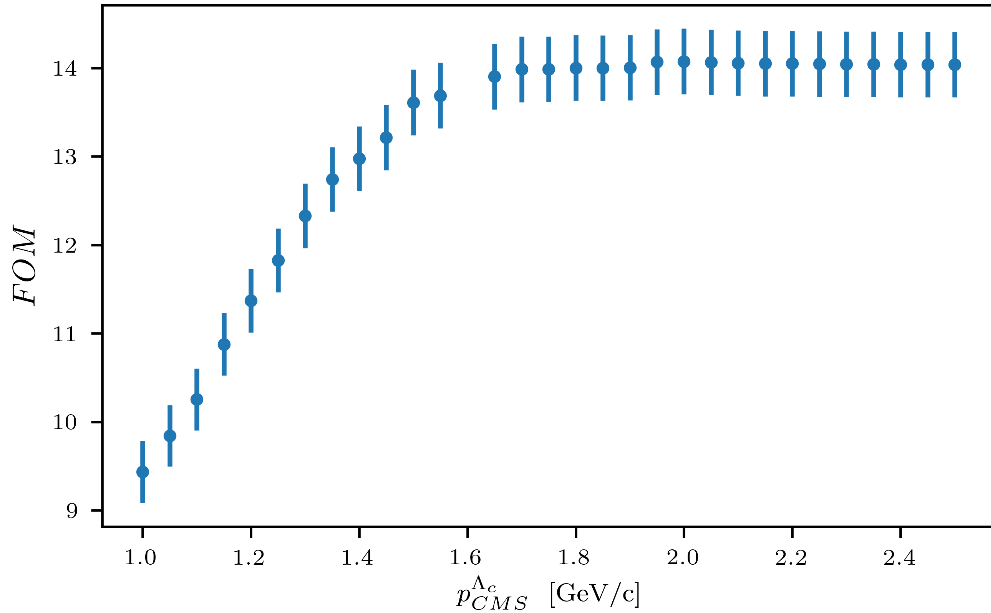


Figure (2.20) Figure of Merit values calculated at several cuts on the momentum of the  $\Lambda_c$  candidates in the center of mass system

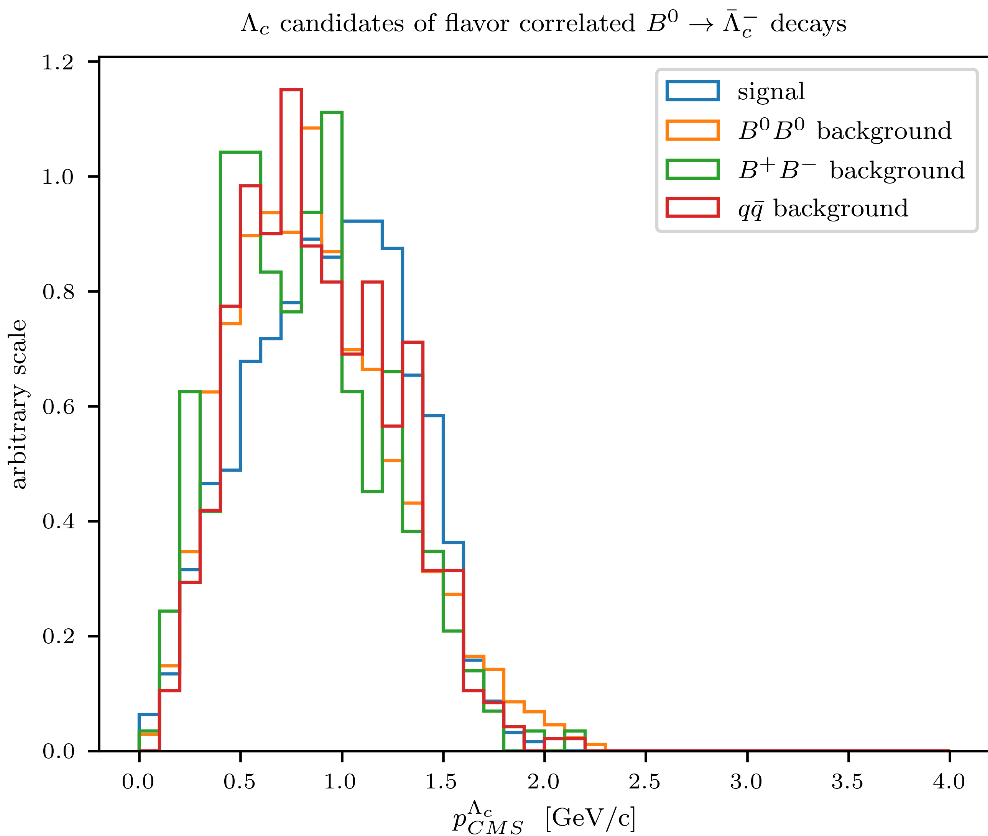


Figure (2.21) Distribution of  $\Lambda_c$  candidates momenta in the center of mass system

164 Fig. 2.22 shows the  $M_{bc}$  and  $M(pK\pi)$  distributions after applying the following set of  
165 cuts:

- 166 •  $foxWolframR2 > 0.3$
- 167 • SignalProbability  $> 0.11$
- 168 •  $p_{CMS}^{\Lambda_c} < 1.7$  GeV/c

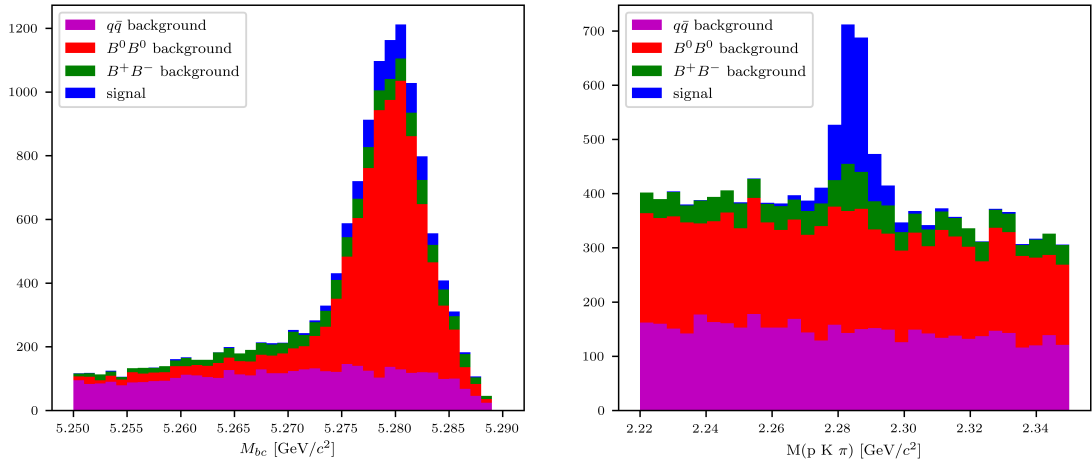


Figure (2.22) Distribution of  $M_{bc}$  (left) and invariant mass of neutral correlated  $\Lambda_c$  candidates (right), in the signal region after the above mentioned selection cuts.

#### **2.4.4 $B^0 \rightarrow \Lambda_c^+ \text{ decays}$**

Finally same procedure is applied also to the neutral anticorrelated decays. The final selections for the variables of *foxWolframR2*, *SignalProbability* and the momentum of the  $\Lambda_c$  candidates in the center of mass system:

- $\text{foxWolframR2} < 0.3$
- $\text{SignalProbability} > 0.15$
- $p_{CMS}^{\Lambda_c} < 1.4 \text{ GeV}/c$

Fig. 2.26 shows the  $M_{bc}$  and  $M(pK\pi)$  distributions after applying these cuts.

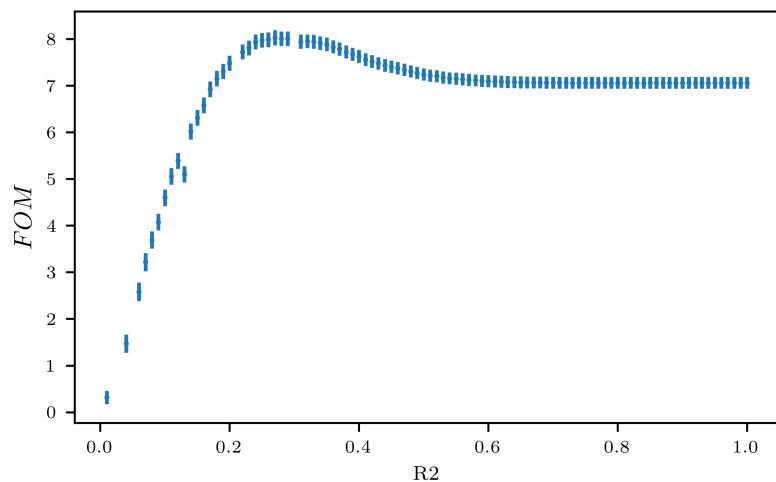


Figure (2.23) Figure of Merit values calculated at several cuts on the *foxWolframR2* variable

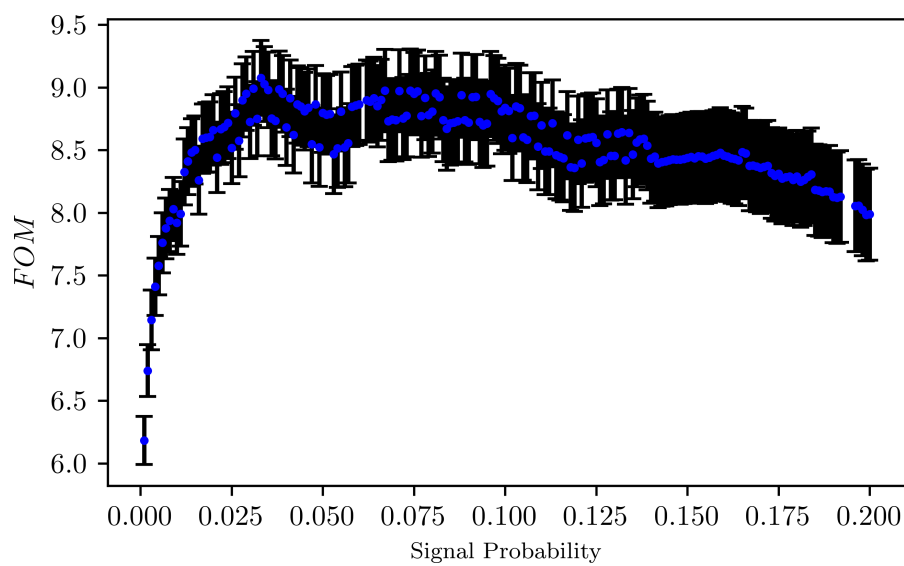


Figure (2.24) Figure of Merit values calculated at several cuts on the *SignalProbability* variable

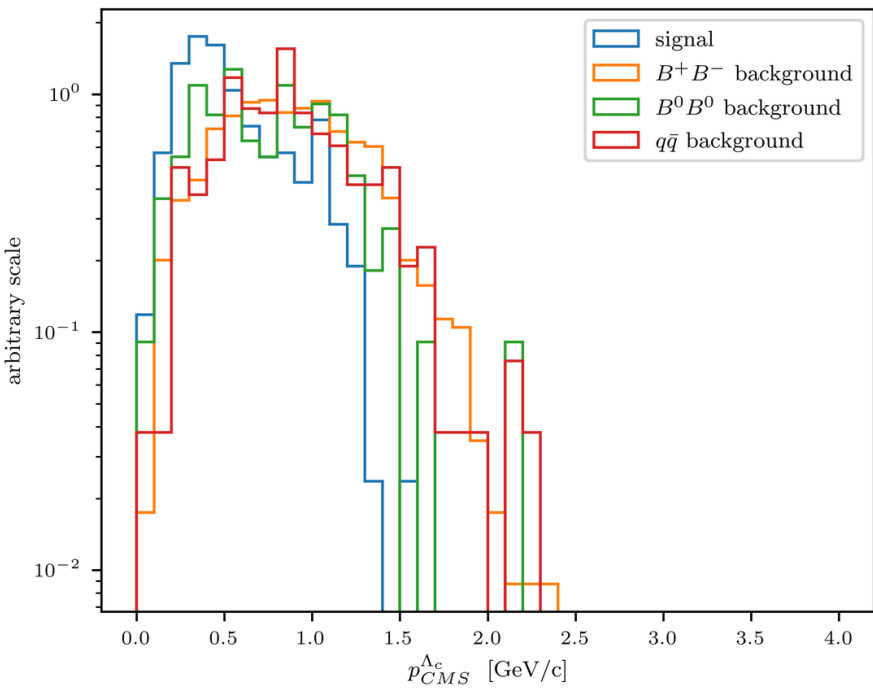


Figure (2.25) Distribution of  $\Lambda_c$  candidates momenta in the center of mass system

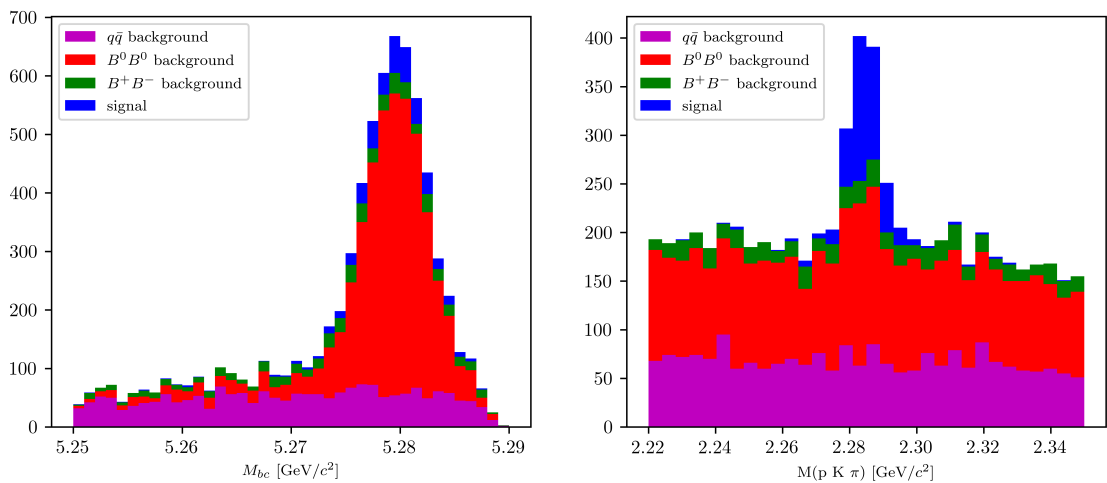


Figure (2.26) Distribution of  $M_{bc}$  (left) and invariant mass of neutral anticorrelated  $\Lambda_c$  candidates (right), in the signal region after the above mentioned selection cuts.

# <sup>177</sup> Chapter 3

## <sup>178</sup> 2D simultaneous fit

### <sup>179</sup> 3.1 Probability Density Functions (PDFs) for the two <sup>180</sup> dimensional fit

<sup>181</sup> The reconstructed events can be categorized as follows:

- <sup>182</sup> peaking in both  $M_{bc}$  and  $M(pK\pi)$
- <sup>183</sup> peaking in  $M_{bc}$  but not in  $M(pK\pi)$
- <sup>184</sup> peaking in  $M(pK\pi)$  but not in  $M_{bc}$
- <sup>185</sup> flat in both  $M_{bc}$  and  $M(pK\pi)$

<sup>186</sup> The first category is represented by the reconstructed signal: signal events which are  
<sup>187</sup> correctly reconstructed. The signal events which are misreconstructed fall into the third  
<sup>188</sup> category. The sum of the two is the so called "total signal". The PDFs used to describe  
<sup>189</sup> the total signal distributions are discussed first.

#### <sup>190</sup> 3.1.1 Total Signal fits

<sup>191</sup> For all the decays, the final sample of total signal events presents a peak around the  
<sup>192</sup> expected  $B$  meson mass and a tail at low  $M_{bc}$  values.

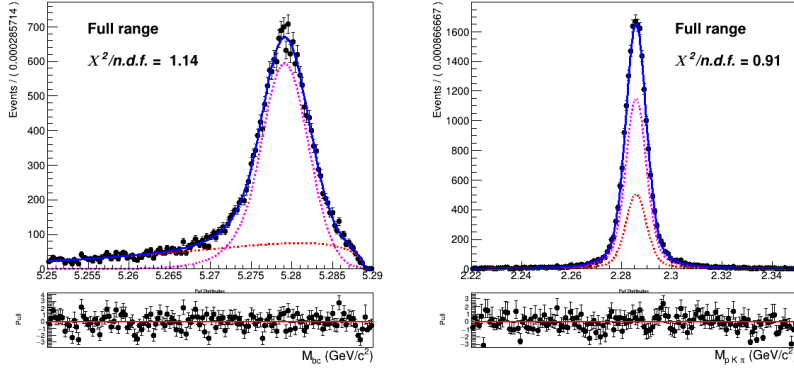


Figure (3.1) Two dimensional fit of charged correlated total signal events in  $M_{bc}$  and  $M(pK\pi)$

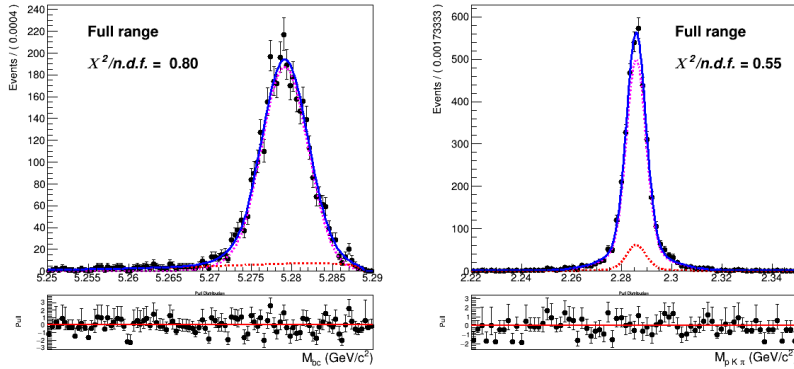


Figure (3.2) Two dimensional fit of charged anticorrelated total signal events in  $M_{bc}$  and  $M(pK\pi)$

193        The 2D fits shown above are performed on five streams of signal MC with a sum of  
 194        the following probability density functions:

$$P_{B,\Lambda_c}^{recSig}(M_{bc}, M(pK\pi)) = \Gamma_{CB}(M_{bc}) \times \rho_G(M(pK\pi)) \quad (3.1)$$

195         $P_{B,\Lambda_c}^{misSig}(M_{bc}, M(pK\pi)) = \Gamma_{ARG}(M_{bc}) \times \rho_G(M(pK\pi)) \quad (3.2)$

196        The first is used to fit the reconstructed signal and  $\Gamma_{CB}(M_{bc})$  is a Crystal Ball function.  
 197        The second is used to model the misreconstructed signal and  $\Gamma_{ARG}(M_{bc})$  is an Argus  
 198        function. In both cases a sum of three Gaussian functions  $\rho_G(M(pK\pi))$  describes the  
 199        mass of the  $\Lambda_c$  baryon.

200        As already said, only the events of reconstructed signal are considered as signal, while  
 201        the misreconstructed signal is considered as background.

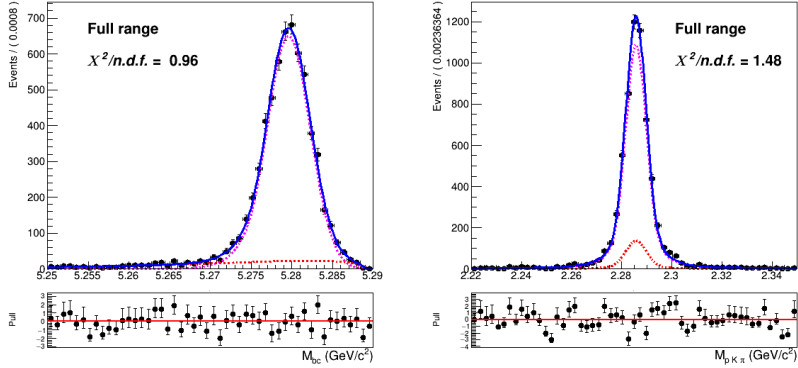


Figure (3.3) Two dimensional fit of neutral correlated total signal events in  $M_{bc}$  and  $M(pK\pi)$

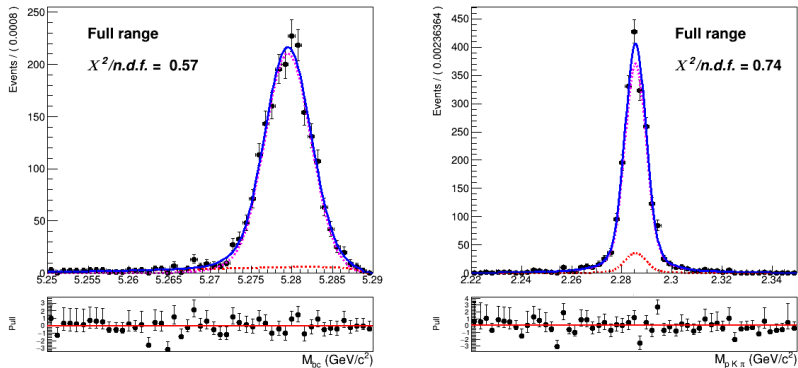


Figure (3.4) Two dimensional fit of neutral anticorrelated total signal events in  $M_{bc}$  and  $M(pK\pi)$

### 3.1.2 $M_{bc}$ peaking and flat background

The background composed of  $B\bar{B}$  events where no  $\Lambda_c$  baryon is produced, is flat in its invariant mass, but can be distinguished in the following two categories:

- peaking in  $M_{bc}$  but not in  $M(pK\pi)$
- flat in both  $M_{bc}$  and  $M(pK\pi)$

as one can see in the following plots.

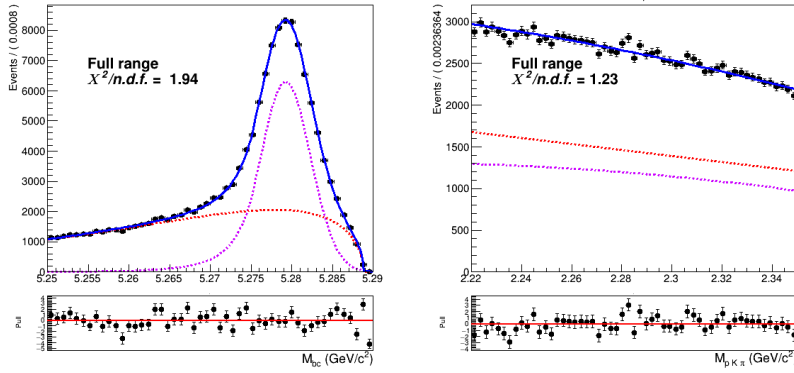


Figure (3.5) Two dimensional fit of charged correlated  $B\bar{B}$  events in  $M_{bc}$  and  $M(pK\pi)$

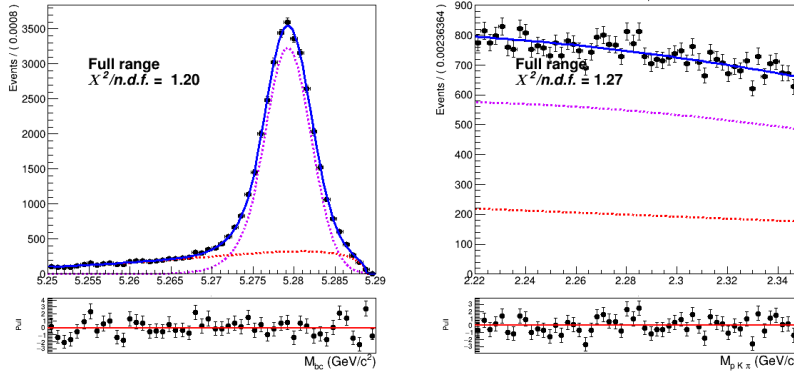


Figure (3.6) Two dimensional fit of charged anticorrelated  $B\bar{B}$  events in  $M_{bc}$  and  $M(pK\pi)$

209 This background presents a similar shape of the distribution in  $M_{bc}$ : the probability  
210 density functions used for it are again a Crystal Ball and an Argus.

211 The two types of background (peaking/flat in  $M_{bc}$ ) are described by:

$$P_{B,\Lambda_c}^{peaking}(M_{bc}, M(pK\pi)) = \Gamma_{CB}(M_{bc}) \times \rho_{Cheb(a_0,a_1)}(M(pK\pi)) \quad (3.3)$$

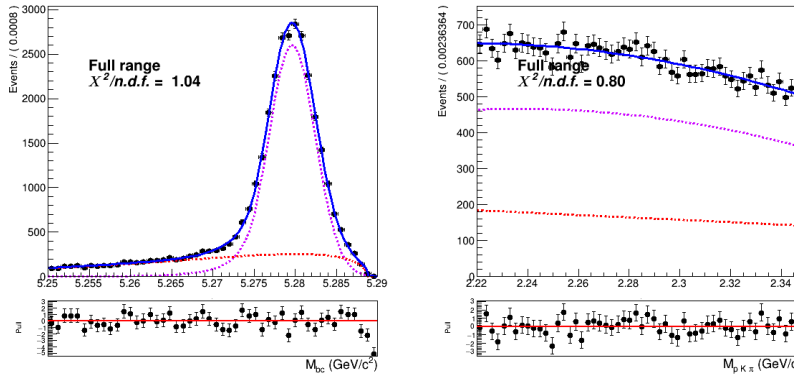


Figure (3.7) Two dimensional fit of neutral correlated  $B\bar{B}$  events in  $M_{bc}$  and  $M(pK\pi)$

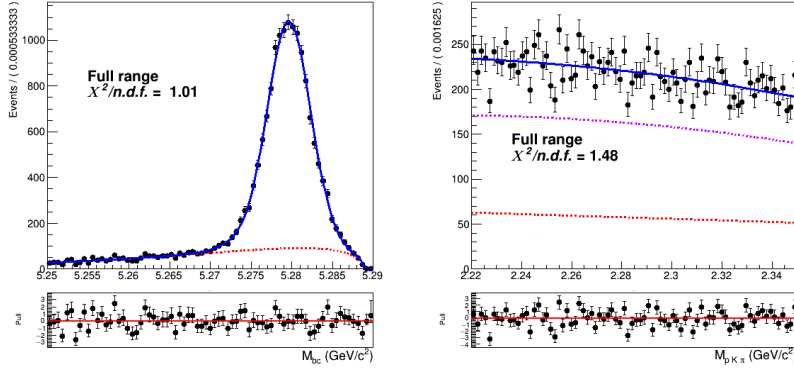


Figure (3.8) Two dimensional fit of neutral anticorrelated  $B\bar{B}$  events in  $M_{bc}$  and  $M(pK\pi)$

$$P_{B,\Lambda_c}^{flat}(M_{bc}, M(pK\pi)) = \Gamma_{ARG}(M_{bc}) \times \rho_{Cheb(b0)}(M(pK\pi)) \quad (3.4)$$

212  
213 where  $\rho_{Cheb(a0,a1)}(M(pK\pi))$  and  $\rho_{Cheb(b0)}(M(pK\pi))$  represent a second order and first order  
214 Chebychev polynomial function respectively.

### 215 3.1.3 Crossfeed background

216 The contamination of misreconstructed  $B^0 \rightarrow \Lambda_c$  events in the  $B^+$  signal (and vice-versa)  
217 induces a background peaking in  $M(pK\pi)$ , but it also slightly peaks near the  $B$  meson  
218 mass, as one can see in Fig. 3.9

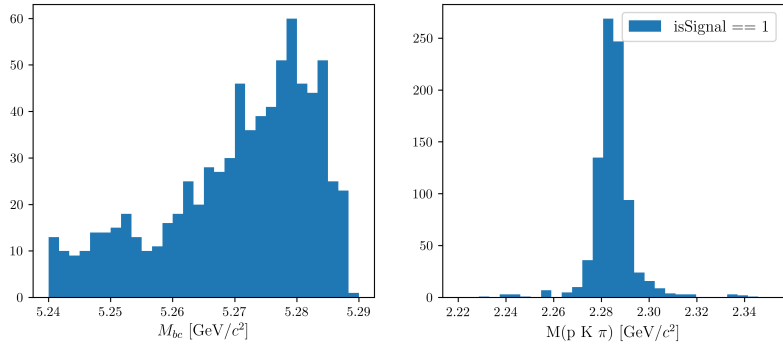


Figure (3.9) Crossfeed distribution in  $M_{bc}$  and  $M(pK\pi)$

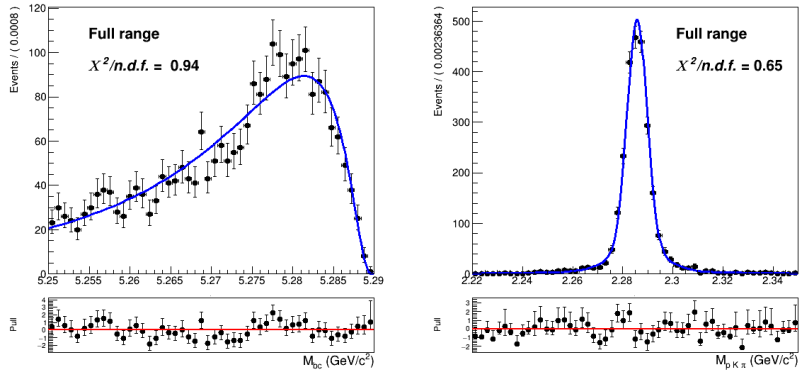


Figure (3.10) Two dimensional fit of crossfeed events in charged correlated channel in  $M_{bc}$  and  $M(pK\pi)$

219 The 2D fit shown above are performed on five streams of signal MC with a sum of the

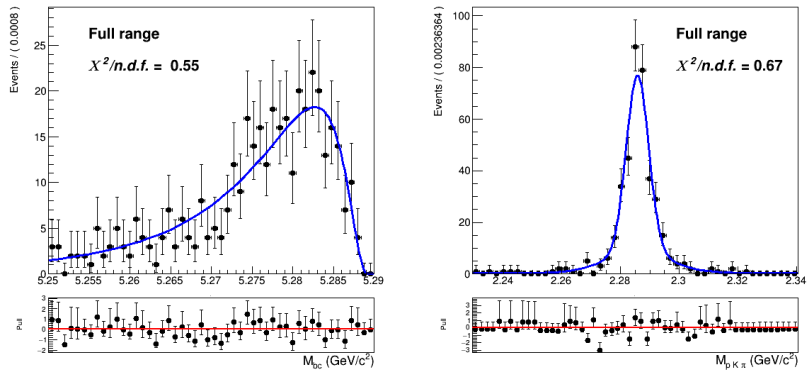


Figure (3.11) Two dimensional fit of crossfeed events in charged anticorrelated channel in  $M_{bc}$  and  $M(pK\pi)$

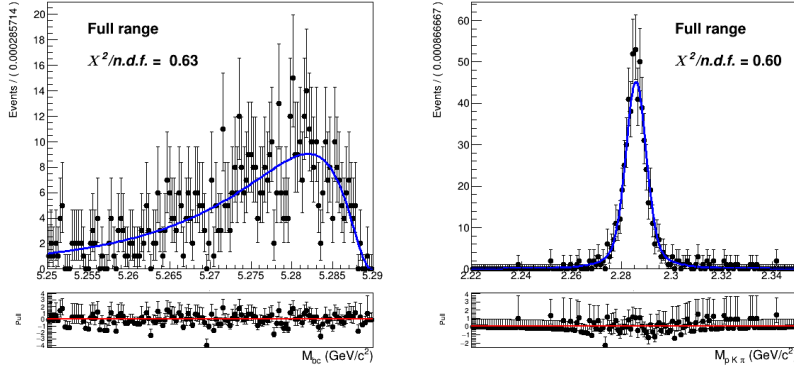


Figure (3.12) Two dimensional fit of crossfeed events in neutral correlated channel in  $M_{bc}$  and  $M(pK\pi)$

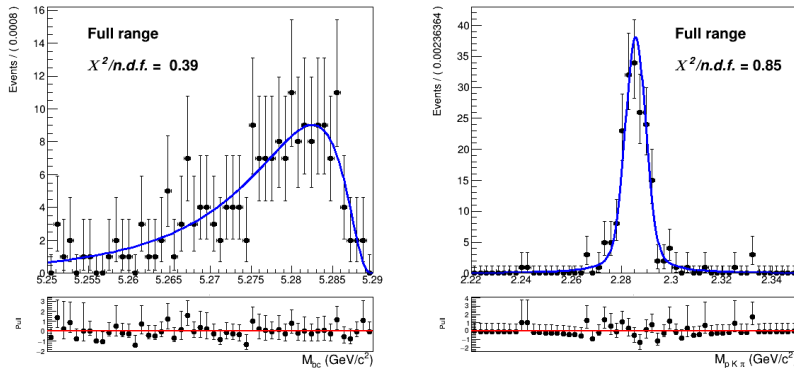


Figure (3.13) Two dimensional fit of crossfeed events in neutral anticorrelated channel in  $M_{bc}$  and  $M(pK\pi)$

following probability density function:

$$P_{B,\Lambda_c}^{Crossfeed}(M_{bc}, M(pK\pi)) = \Gamma_{Novosibirsk}(M_{bc}) \times \rho_G(M(pK\pi)) \quad (3.5)$$

where  $\Gamma_{Novosibirsk}(M_{bc})$  is a Novosibirsk function and the mass of the  $\Lambda_c$  baryon is described by the same sum of three Gaussian functions  $\rho_G(M(pK\pi))$  as in Eq.3.1.

### 3.1.4 Continuum background

Besides the dataset recorded at the energy of the  $\Upsilon(4S)$  resonance ( $E_{CMS}^{on-res} = 10.58$  GeV), the *Belle* experiment recorded a sample of  $89.4 \text{ fb}^{-1}$  at an energy 60 MeV below the nominal  $\Upsilon(4S)$  resonance ( $E_{CMS}^{off-res} = 10.52$  GeV). The dataset allows to check for an appropriate modeling of the continuum MC simulation. Using the official tables (<https://belle.kek.jp/secured/nbb/nbb.html>) the off-resonance sample is scaled by

$$\frac{\mathcal{L}^{on-res}}{\mathcal{L}^{off-res}} \left( \frac{E_{CMS}^{off-res}}{E_{CMS}^{on-res}} \right)^2 \quad (3.6)$$

229 taking into account the difference in luminosity and in  $E_{CMS}$  (Energy in center of mass  
230 system).

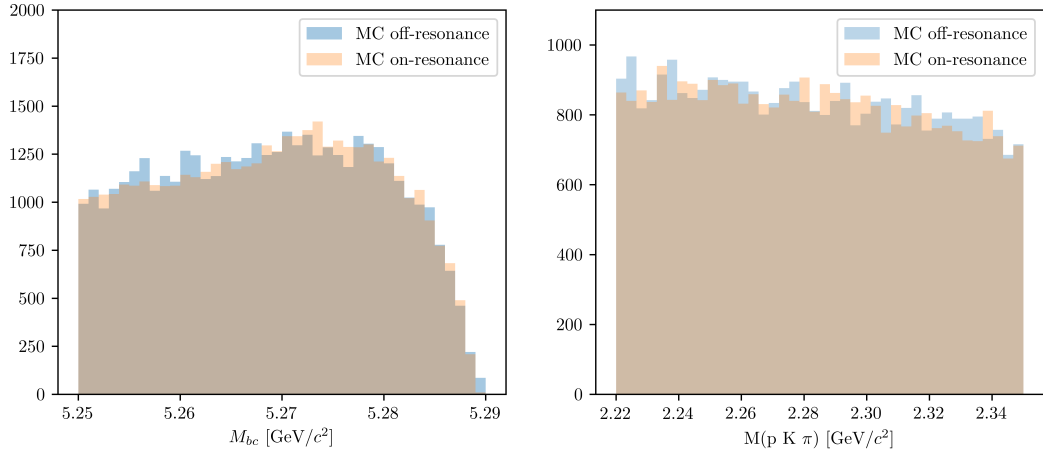


Figure (3.14)  $M_{bc}$  and  $M(pK\pi)$  comparison between on-/off-resonance (scaled) Monte Carlo simulated continuum. The scaling is applied according to Eq. (3.6) and shifting the  $M_{bc}$  distribution by  $E_{CMS}^{on-res} - E_{CMS}^{off-res}$ .

231 The plot in Fig.3.14 shows the  $M_{bc}$  and  $M(pK\pi)$  distributions in the MC on-/off-resonance  
232 continuum after the scaling<sup>1</sup>.

233 Ideally, provided that there's a good agreement between MC and data for the off-  
234 resonance sample and also between the MC on-/off-resonance continuum after the scaling,  
235 one could directly use the scaled off-resonance data to describe the continuum background  
236 in the fit on data. There are two reasons that prevent this very straightforward approach:

- 237 • First, since the off-resonance MC (and data) present very low statistics (Fig. 3.15a  
238 shows the  $\Lambda_c$  invariant mass in off-resonance data), scaling them with all the applied  
239 selection cuts would cause the PDF describing the continuum to be very much  
240 affected by statistical fluctuations.
- 241 • Secondly, the  $B$  meson candidates are reconstructed in both on-resonance and off-  
242 resonance events for values of  $M_{bc} \geq 5.22 \text{ GeV}/c^2$ , but the  $E_{CMS}$  differs: there can be  
243 effects of correlations between the applied *SignalProbability* cut and the  $M_{bc}$  variable  
244 that one needs to take into account.

---

244<sup>1</sup>it is obtained with the MC off-resonance sample being composed of 6 streams: the total amount is normalized

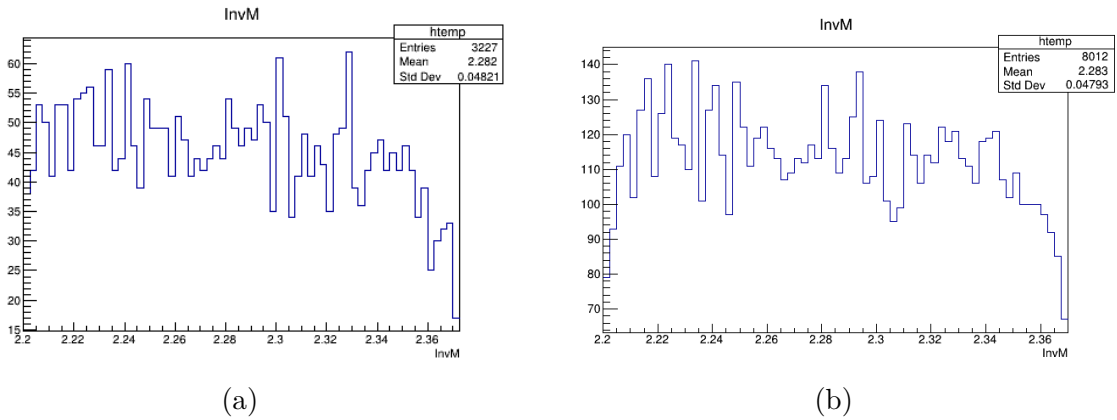


Figure (3.15) On the left:  $\Lambda_c$  invariant mass in off-resonance data (all nominal cuts applied). On the right:  $\Lambda_c$  invariant mass in off-resonance data after the continuum suppression cut removal.

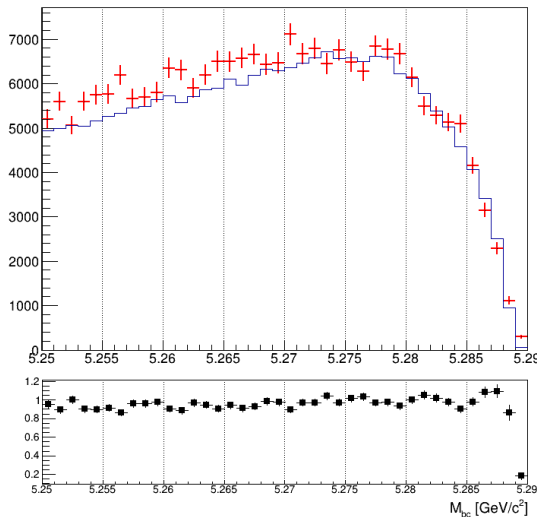


Figure (3.16)  $M_{bc}$  distributions of the MC (scaled) off-resonance sample (in red) and on-resonance (in blue) using 5 streams statistics and all nominal selection cuts applied.

245 In Fig. 3.16 one can notice some discrepancy in the shapes, apart from the not negligible  
246 statistical fluctuations in the (scaled) off-resonance distribution.

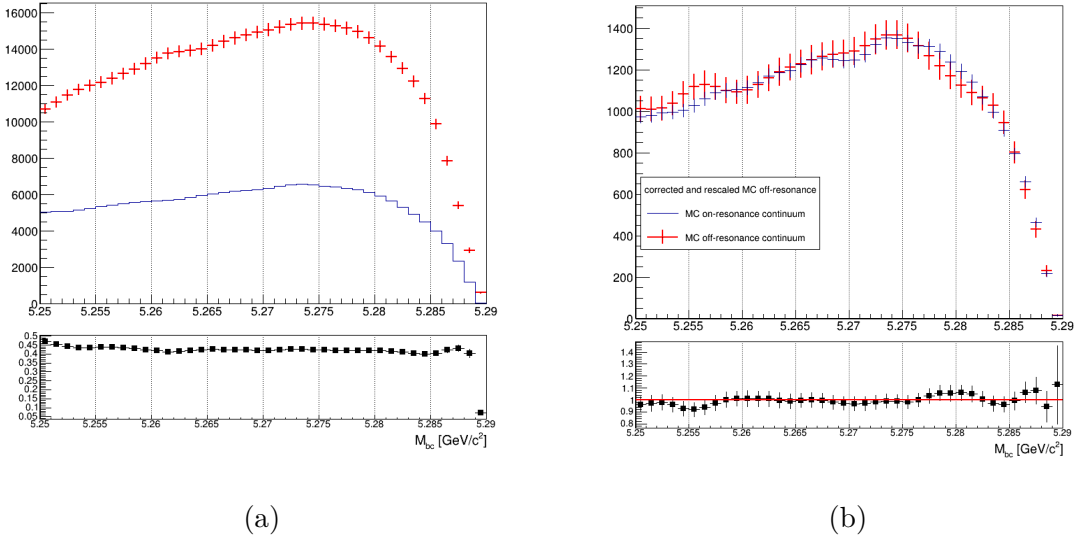
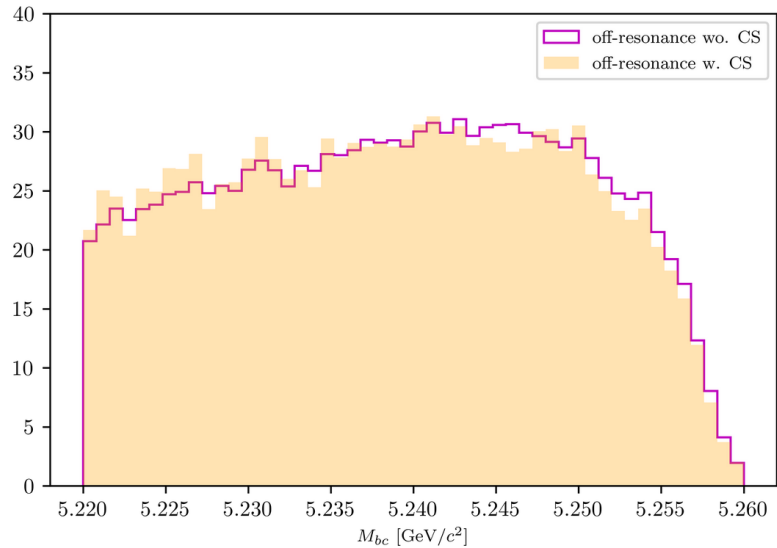


Figure (3.17) On the left:  $M_{bc}$  distributions of the MC off-resonance sample without continuum suppression and the MC continuum sample with applied continuum suppression. On the right:  $M_{bc}$  distributions of the corrected scaled MC off-resonance and on-resonance MC continuum.

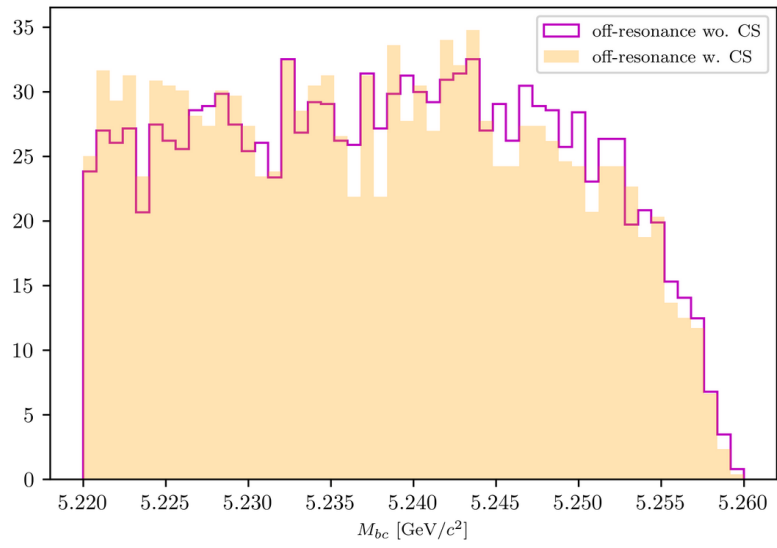
247     The procedure adopted to obtain the PDF describing the continuum background  $M_{bc}$   
248     distribution is the following:

- 249     • 5 streams of off-resonance MC were scaled according to Eq. (3.6) without continuum  
250       suppression being applied and compared to the distribution of 5 streams of on-  
251       resonance continuum
- 252     • From a ratio plot, like the one in Fig. 3.17a, the bin-correction is obtained to  
253       correct the off-resonance data in the scaling procedure. To obtain the shape that  
254       can describe the continuum background  $M_{bc}$  distribution on data the continuum  
255       suppression is not applied on the off-resonance continuum sample, in order to acquire  
256       more statistics.

257     This procedure is first tested on an independent MC sample (see Fig. 3.17b ) to check the  
258     result on simulated data before applying it on data.



(a)



(b)

Figure (3.18) Above:  $M_{bc}$  distributions of the MC off-resonance sample (5 streams) with and without continuum suppression. Below:  $M_{bc}$  distributions on data with and without continuum suppression.

- The validity of the method relies on the fact that the difference between on-/off-resonance continuum events are well modeled in MC and that the shape of the  $M_{bc}$  distribution doesn't change significantly when removing the continuum suppression cut both on MC and data (as one can see from Figures 3.18a - 3.18b). Additionally, the continuum suppression cut efficiency should be the same in data and MC in order to have the correct scaling on data with the above mentioned method. Fig.

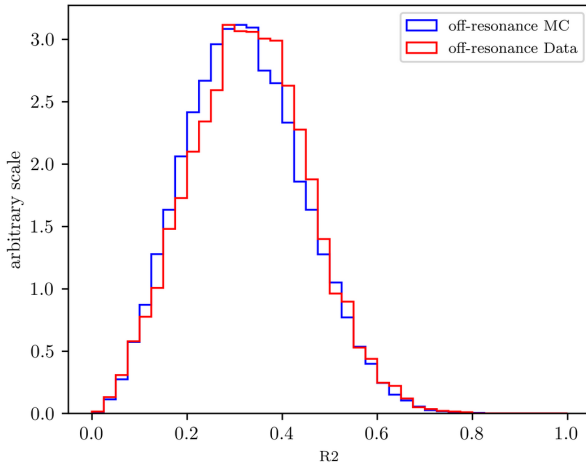


Figure (3.19) Distributions of variable *foxWolframR2* in off-resonance MC and data.

3.19 shows the distribution of the *foxWolframR2* variable in off-resonance MC and data. The slight shift visible in data can cause a different impact on data in terms of rejected continuum background when applying the  $\text{foxWolframR2} < 0.3$  cut. It is found to reject about 60% of the continuum background in data, whereas it rejects 55% of the continuum background in MC ( 56% in on-resonance MC). Therefore in data one can expect about 2.25% less continuum background events. This discrepancy is not statistically significant (the statistical uncertainty for the continuum background events is of the level of  $\sim 1\%$ ), a simple correction to the number of events can be applied on data and its possible systematics can be then taken into account.  
The obtained distribution can be then fitted with a Novosibirsk function (see Fig. 3.20). This is the procedure which can be then applied on the off-resonance data to obtain the  $M_{bc}$  shape describing the continuum background in data.

In the  $\Lambda_c$  invariant mass one doesn't expect correlation effects, but nevertheless there can be differences due to the limited statistics of the off-resonance sample. In fact, in the case of on-resonance MC for the charged correlated decays some events in which  $\Lambda_c$  candidates survive nominal selection cuts are visible and can be described with a small Gaussian on the top of the flat background (Fig.3.21a). Due to the low statistics one cannot see a similar peak in the off-resonance sample (the Fig.3.21b shows a 5 streams statistics).

The shape describing the  $\Lambda_c$  invariant mass in the case of charged correlated decays is obtained from the simulated on-resonance continuum, again using 5 streams statistics (see Fig. 3.21a ). In the other cases no peak is visible and therefore also the  $\Lambda_c$  invariant mass shape is obtained from 5 streams of off-resonance events.

Finally, it is possible to examine the validity of the whole procedure on the independent stream. Fig. 3.22 - 3.25 show the  $M_{bc}$ ,  $M(pK\pi)$  projections of the overlayed two dimensional PDFs obtained with the above described procedure.

The 2D PDF used for Fig. 3.22 can be written as:

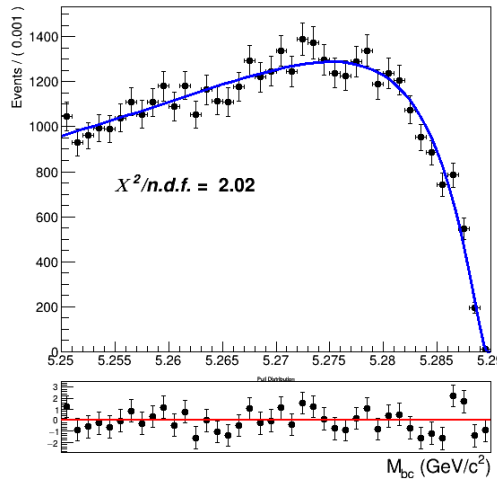


Figure (3.20) Fit of the  $M_{bc}$  distribution MC (scaled) off-resonance continuum (one stream).

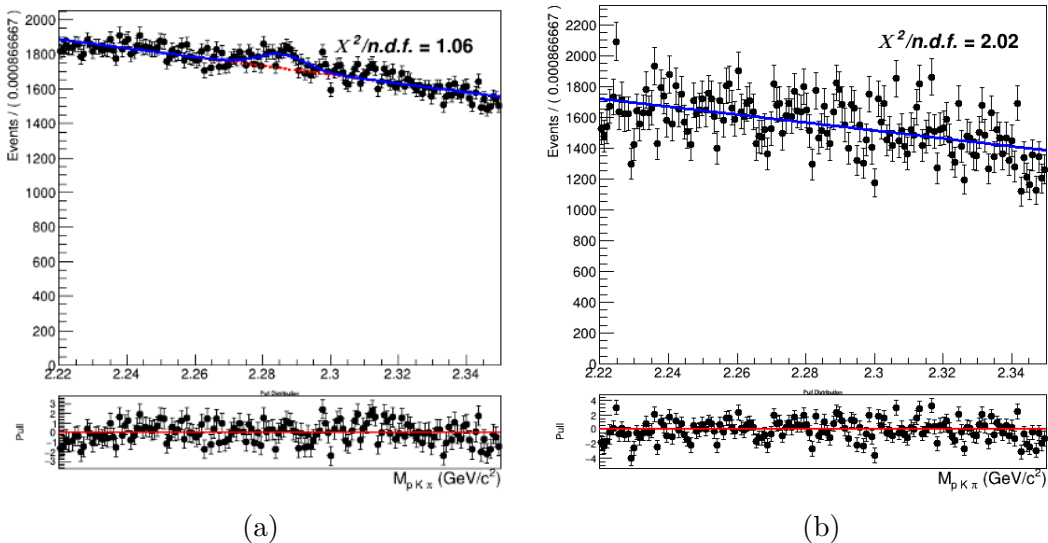


Figure (3.21) Comparison between 5 streams of MC on-resonance continuum 3.21a) and off-resonance (scaled) continuum in  $M(pK\pi)$  (3.21b).

292

$$P_{B,\Lambda_c}^{Continuum}(M_{bc}, M(pK\pi)) = \Gamma_{Nov}(M_{bc}) \times [\rho_{Cheb1}(M(pK\pi)) + \rho_G(M(pK\pi))]$$

294

295 where, as already anticipated, the invariant mass is described by a sum of a first order  
 296 Chebychev polynomial and the peak by the same triple Gaussian PDF adopted for the  
 297 signal. The 2D PDF used for Fig. 3.23 and Fig. 3.24 differ only in the invariant mass, not  
 298 having the triple gaussian. Whereas the 2D PDF used for Fig. 3.25 can be written as:

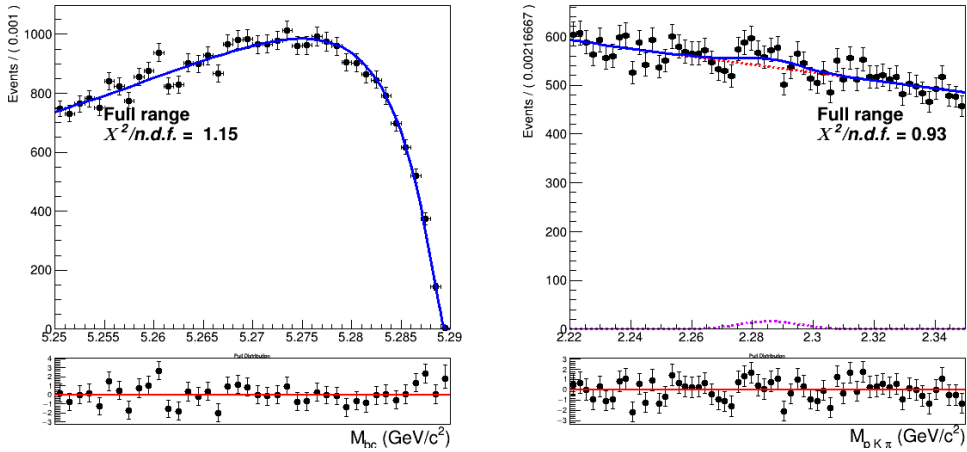


Figure (3.22) Two dimensional fit of charged correlated continuum events (one stream).

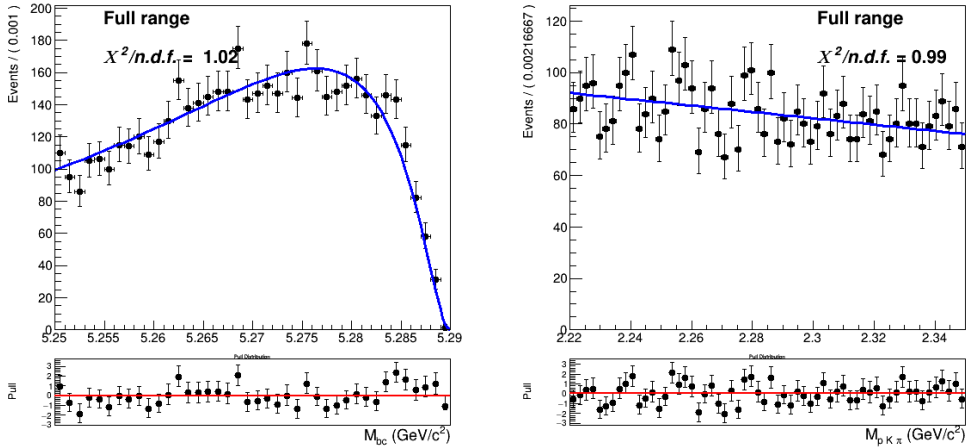


Figure (3.23) Two dimensional fit of charged anticorrelated continuum events (one stream).

299

$$300 \quad P_{B,\Lambda_c}^{Continuum}(M_{bc}, M(pK\pi)) = \Gamma_{Argus}(M_{bc}) \times [\rho_{Cheb1}(M(pK\pi)]$$

301

302 since the distribution in  $M_{bc}$  can be better described by an Argus.

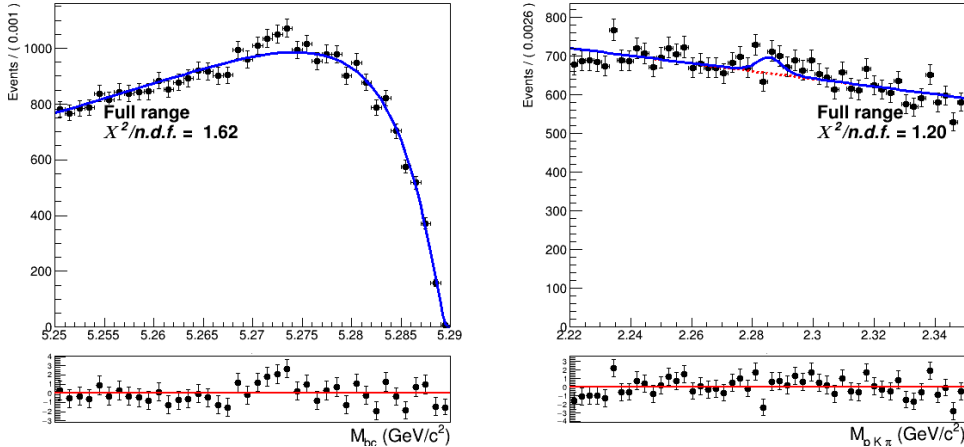


Figure (3.24) Two dimensional fit of continuum events (one stream).

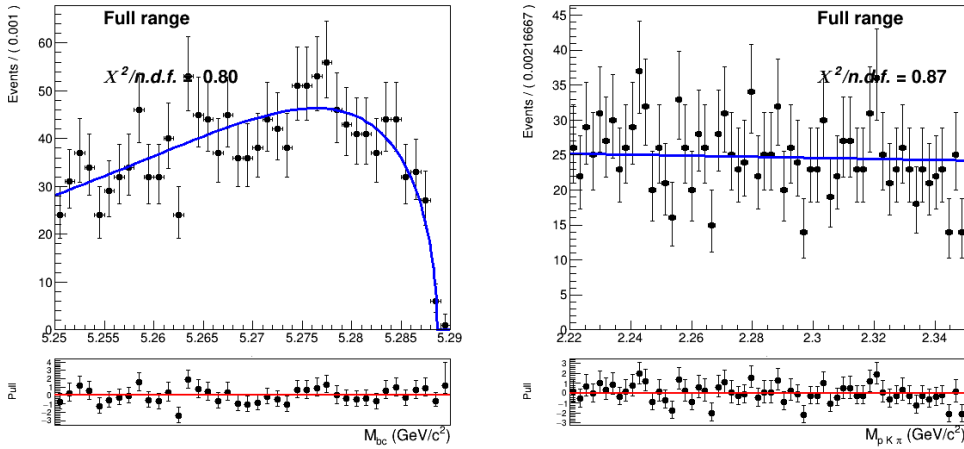


Figure (3.25) Two dimensional fit of continuum events (one stream).

## 3.2 Two dimensional fit on Monte Carlo

A total of six independent streams were used to construct/validate the fit model: each time five streams were used to construct the already discussed PDFs and the independent stream is used to test if the total PDF enables to extract the signal yield in an unbiased way (a total of six fits are performed on the six different streams of generic MC). To especially suppress the systematic uncertainties deriving from the amount of crossfeed the samples corresponding to the four different decay channels are fitted simultaneously. In all six fits all the shaping parameters are kept fixed, except:

- $\sigma_{G1}$ : the width of the main of the three Gaussian functions in  $\rho_G(M(pK\pi))$
- $\sigma_{CB}$  parameter for the Crystal Ball describing the signal peak in  $M_{bc}$

313 In the  $M_{bc}$  distribution the  $\sigma_{CB}$  width parameter for the Crystal Ball describing the  $M_{bc}$   
 314 peaking background is expressed as function of the signal  $\sigma_{CB}$  with a ratio fixed from MC.  
 315 As for the normalizations, mis-/reconstructed signal events and  $M_{bc}$  peaking/flat back-  
 316 ground events are floated in the two dimensional unbinned maximum likelihood fits.  
 317 The continuum background normalization is kept fixed to the value obtained by the  
 318 off-resonance scaling procedure.  
 319 Instead, the normalization of crossfeed background events is determined by the fit in the  
 320 following way:

$$N_{CrossBkg} = N_{recSig}^{corr} \cdot (\epsilon_{cross}/\epsilon_{recSig})^{corr} + N_{recSig}^{anticorr} \cdot (\epsilon_{cross}/\epsilon_{recSig})^{anticorr} \quad (3.7)$$

321 where  $N_{recSig}^{corr}$  ( $N_{recSig}^{anticorr}$ ) are the fitted signal yields of the corresponding crossfeeding  
 322 decay and  $(\epsilon_{cross}/\epsilon_{recSig})$  are the ratios of misreconstruction efficiency and signal recon-  
 323 struction efficiency as determined in the Monte Carlo. Since the crossfeed can likely  
 324 occur both from correlated and anticorrelated channels, both are considered and summed  
 325 together.

326 Exemplary, the distributions of stream 0 overlaid by the fitted PDF are depicted in  
 327 Figs. 3.27 to 3.37. In Tables 3.1 to 3.4 the signal yields of the fits (**Reconstructed**  
 328 **Signal**) to the two dimensional distributions for the six streams are listed and compared  
 329 to the yields obtained from fits of signal distributions of each individual stream. The  
 330 latter are the "expected" yields of reconstructed signal from a fit to the total signal events  
 331 in the individual stream as the one plotted on Fig. 3.26 where all the parameters of the  
 332 PDFs described in Eq. (3.1) are kept fixed and the corresponding yields are extracted from  
 333 the fit. Note that in the case of Tables Table 3.3 - 3.4 the reconstructed signal yields are  
 334 contaminated by events from the other neutral  $B^0$  decay channel that experience mixing.  
 335 Since those events cannot be analytically distinguished from the true signal events, the  
 336 branching fraction calculation for neutral decays needs to take them into account and  
 337 correct for their contribution (as will be shown in the next Chapter).

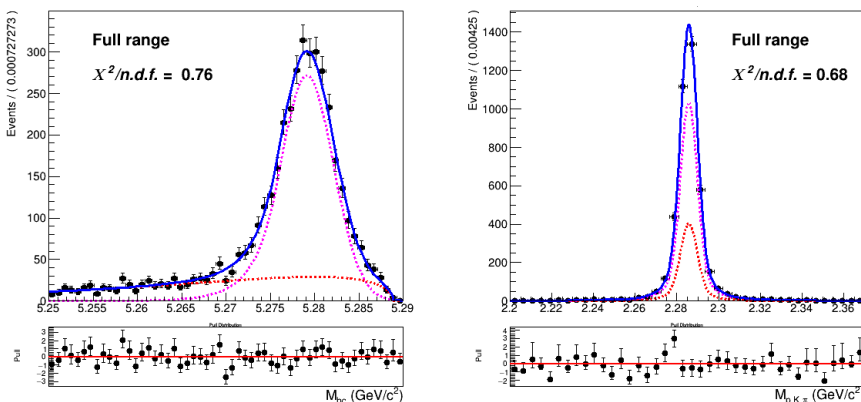


Figure (3.26) Two dimensional fit of Total Signal of stream 0 used to extract the expected reconstructed (corresponding to the PDF colored in magenta) and expected misreconstructed yields (corresponding to the PDF colored in red).

<sup>338</sup> 3.2.1 Fit results for  $B^- \rightarrow \Lambda_c^+ \text{ decays}$

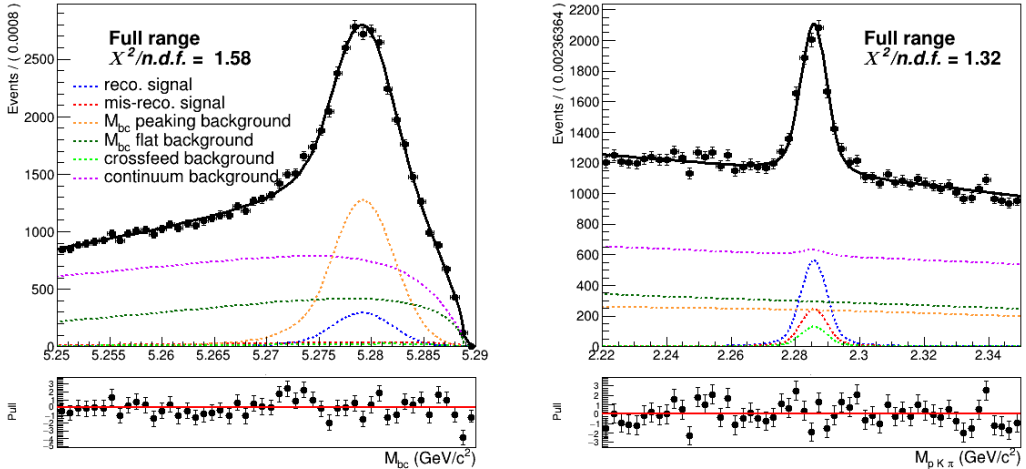


Figure (3.27) Projections of the two dimensional simultaneous fit on stream 0 Monte Carlo simulated data for charged correlated decays.

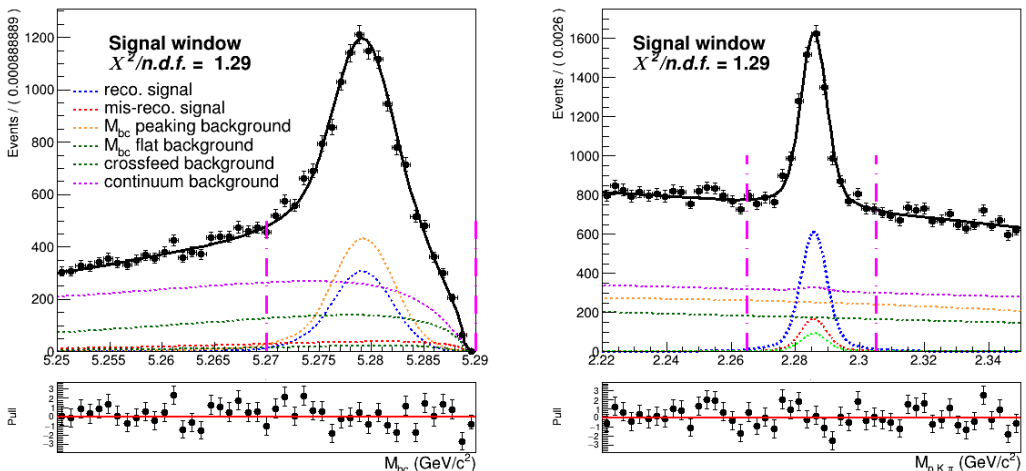


Figure (3.28) Projections of the two dimensional simultaneous fit on stream 0 Monte Carlo simulated data for charged correlated decays(in the signal window)

	Reconstructed Signal		Total Signal			
	fit	expected	fit	MC truth	fit - MC truth	
stream 0	$2829 \pm 130$	$2928 \pm 66$	$4063 \pm 157$	4061	-2	-0.05%
stream 1	$2811 \pm 137$	$2956 \pm 65$	$4095 \pm 161$	4084	11	0.3%
stream 2	$2952 \pm 141$	$2940 \pm 65$	$4345 \pm 165$	4138	207	5.0%
stream 3	$2747 \pm 134$	$2867 \pm 66$	$4267 \pm 160$	4105	162	3.9%
stream 4	$3043 \pm 138$	$3017 \pm 67$	$4148 \pm 157$	4176	-28	-0.7%
stream 5	$2818 \pm 136$	$2816 \pm 65$	$3999 \pm 162$	4001	-2	-0.05%
sum	17200	17524	24917	24565	348	1.4%

Table (3.1) Charged correlated decays: comparison of fitted and expected signal yields, fitted and truth-matched total signal for six streams of Belle generic MC when fitting the two dimensional distributions of  $M_{bc}$  and  $M(pK\pi)$ .

<sup>339</sup> The yields obtained by the fit show a slight tendency of underestimation, but when  
<sup>340</sup> comparing the sums of them with the sum of expected values one can see the difference is  
<sup>341</sup> within statistical fluctuations ( within 2%).

<sup>342</sup> The tendency of underestimation is visible in , but it is just slightly larger than  $\sigma$

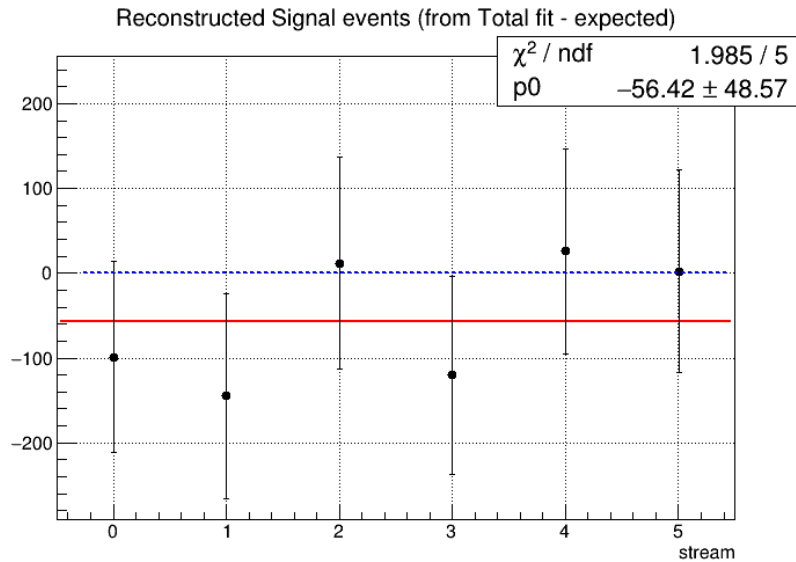


Figure (3.29) Residuals of signal yields (alias reconstructed signal, values reported in the first two columns of the above displayed table).

### 3.2.2 Fit results for $B^- \rightarrow \bar{\Lambda}_c^-$ decays

For the anticorrelated decays from charged  $B$  mesons the slight tendency is in the opposite direction. But the distribution of residuals (see Fig. 3.30) shows this slight overestimation is well within the statistical uncertainty.

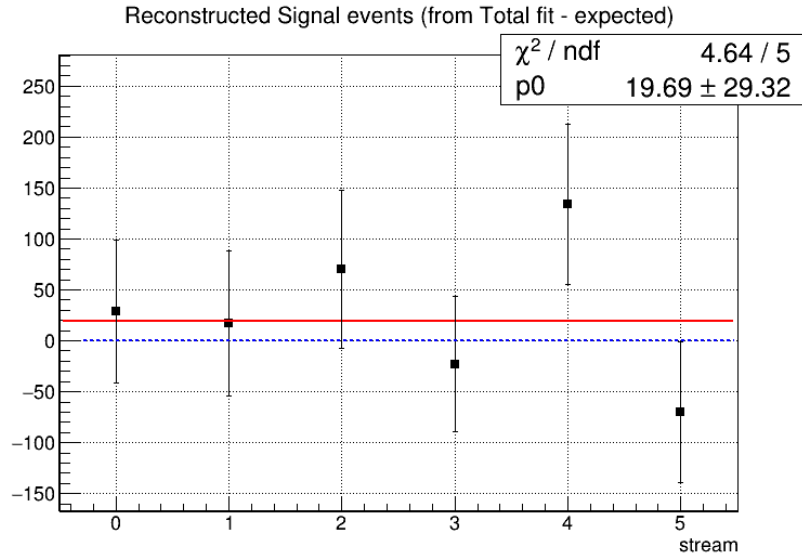


Figure (3.30) Residuals of signal yields (alias reconstructed signal, values reported in the first two columns of the above displayed table).

	Reconstructed Signal		Total Signal			fit - MC truth
	fit	expected	fit	MC truth	fit - MC truth	
stream 0	$724 \pm 64$	$695 \pm 28$	$813 \pm 73$	765	48	6.3%
stream 1	$726 \pm 65$	$709 \pm 29$	$802 \pm 67$	785	17	2.2%
stream 2	$788 \pm 72$	$718 \pm 29$	$911 \pm 72$	797	114	14.3%
stream 3	$679 \pm 60$	$702 \pm 29$	$768 \pm 66$	802	-34	4.2%
stream 4	$844 \pm 73$	$710 \pm 29$	$982 \pm 73$	785	197	25.1%
stream 5	$605 \pm 63$	$675 \pm 29$	$722 \pm 63$	760	-38	-5.0%
sum	4366	4209	4998	4694	304	6.5%

Table (3.2) Charged anticorrelated decays: comparison of fitted and expected signal yields, fitted and truth-matched total signal for six streams of Belle generic MC when fitting the two dimensional distributions of  $M_{bc}$  and  $M(pK\pi)$ .

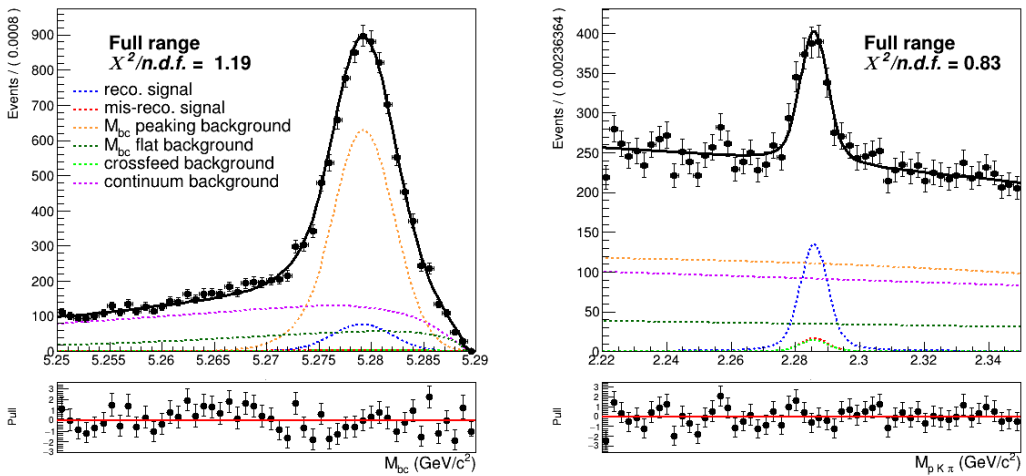


Figure (3.31) Projections of the two dimensional simultaneous fit on stream 0 Monte Carlo simulated data for charged anticorrelated decays.

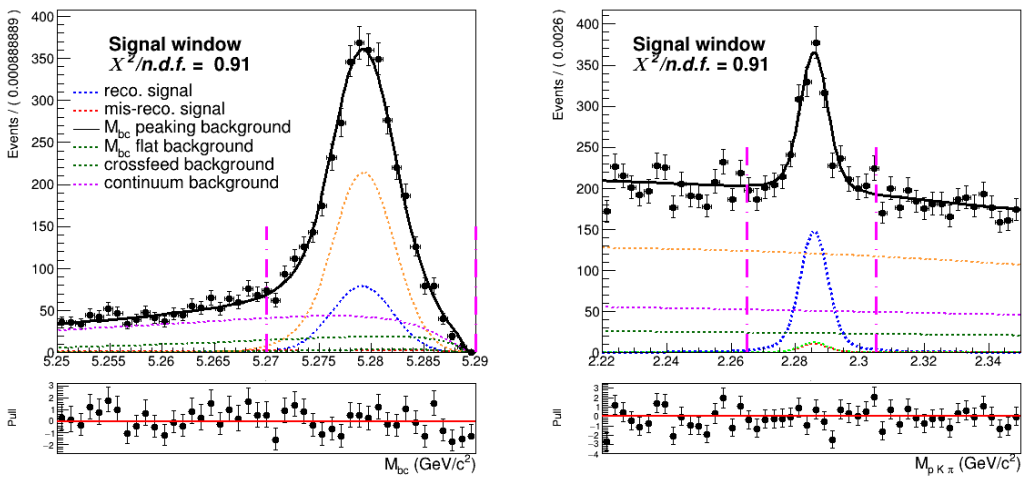


Figure (3.32) Projections of the two dimensional simultaneous fit on stream 0 Monte Carlo simulated data for charged anticorrelated decays (in the signal window).

### <sup>347</sup> 3.2.3 Fit results for $\bar{B}^0 \rightarrow \Lambda_c^+ \text{ decays}$

<sup>348</sup> Also in the case of the neutral correlated one can observe a slight overestimation in the  
<sup>349</sup> reconstructed signal yields. The residuals (see Fig. 3.33) show that this is not so negligible:  
<sup>350</sup> the significance is about  $1.5\sigma$ .

	Reconstructed Signal		Total Signal			
	fit	expected	fit	MC truth	fit - MC truth	
stream 0	$1329 \pm 69$	$1240 \pm 38$	$1390 \pm 70$	1379	11	0.8%
stream 1	$1314 \pm 68$	$1327 \pm 38$	$1319 \pm 66$	1287	14	2.5%
stream 2	$1266 \pm 68$	$1254 \pm 38$	$1273 \pm 65$	1251	22	1.8%
stream 3	$1320 \pm 67$	$1248 \pm 38$	$1316 \pm 66$	1255	35	4.9%
stream 4	$1227 \pm 67$	$1214 \pm 38$	$1300 \pm 66$	1223	77	6.3%
stream 5	$1282 \pm 70$	$1233 \pm 38$	$1251 \pm 66$	1246	5	0.4%
sum	7738	7516	7709	7525	140	1.86%

Table (3.3) Comparison of fitted and expected signal yields, fitted and truth-matched total signal for six streams of Belle generic MC when fitting the two dimensional distributions of  $M_{bc}$  and  $M(pK\pi)$ .

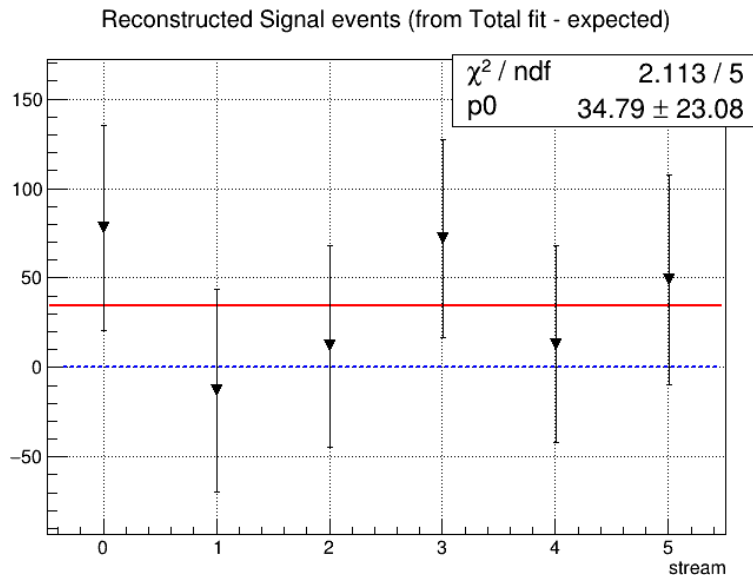


Figure (3.33) Residuals of signal yields for neutral correlated decays.

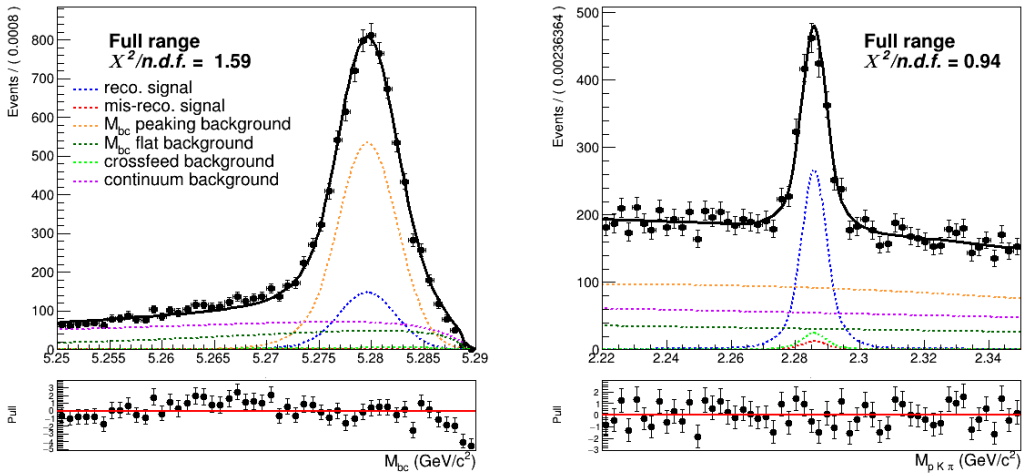


Figure (3.34) Projections of the two dimensional simultaneous fit on stream 0 Monte Carlo simulated data for neutral correlated decays.

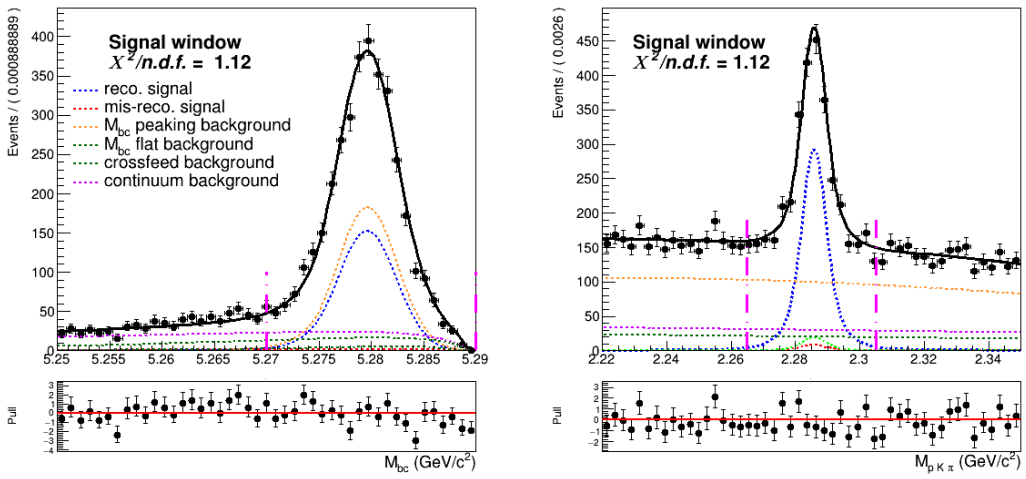


Figure (3.35) Projections of the two dimensional simultaneous fit on stream 0 Monte Carlo simulated data for neutral correlated decays.

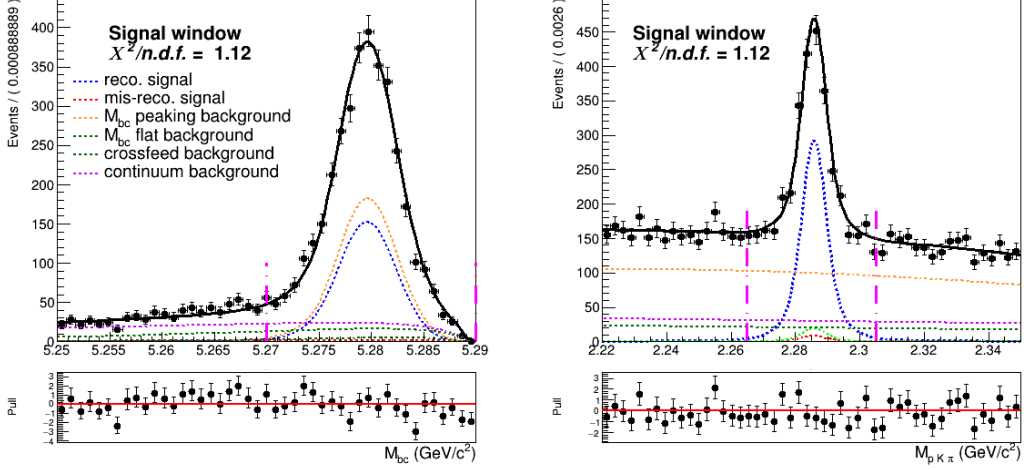


Figure (3.36) Projections of the two dimensional simultaneous fit on stream 0 Monte Carlo simulated data for neutral correlated decays (in the signal window).

### <sup>351</sup> 3.2.4 Fit results for $\bar{B}^0 \rightarrow \bar{\Lambda}_c^-$ decays

	Reconstructed Signal		Total Signal			
	fit	expected	fit	MC truth	fit - MC truth	
stream 0	$567 \pm 45$	$575 \pm 29$	$657 \pm 45$	668	-11	-1.6%
stream 1	$565 \pm 46$	$607 \pm 21$	$660 \pm 47$	687	-27	-3.9%
stream 2	$574 \pm 46$	$593 \pm 20$	$659 \pm 45$	639	20	3.1%
stream 3	$714 \pm 49$	$596 \pm 21$	$792 \pm 52$	680	112	16.4%
stream 4	$603 \pm 50$	$594 \pm 21$	$693 \pm 50$	638	55	8.6%
stream 5	$589 \pm 63$	$595 \pm 21$	$603 \pm 44$	624	-21	3.4%
sum	3612	3560	4064	3936	170	4.3%

Table (3.4) Neutral anticorrelated decays: comparison of fitted and expected signal yields, fitted and truth-matched total signal for six streams of Belle generic MC when fitting the two dimensional distributions of  $M_{bc}$  and  $M(pK\pi)$ .

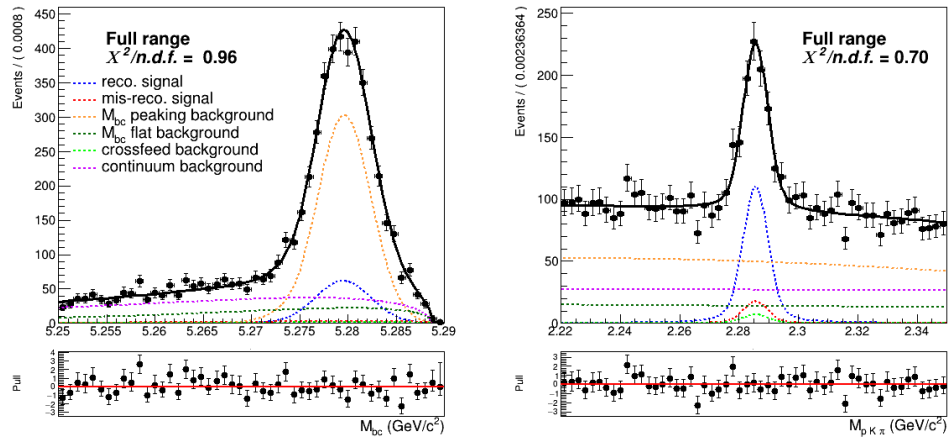


Figure (3.37) Projections of the two dimensional simultaneous fit on stream 0 Monte Carlo simulated data for neutral anticorrelated decays.

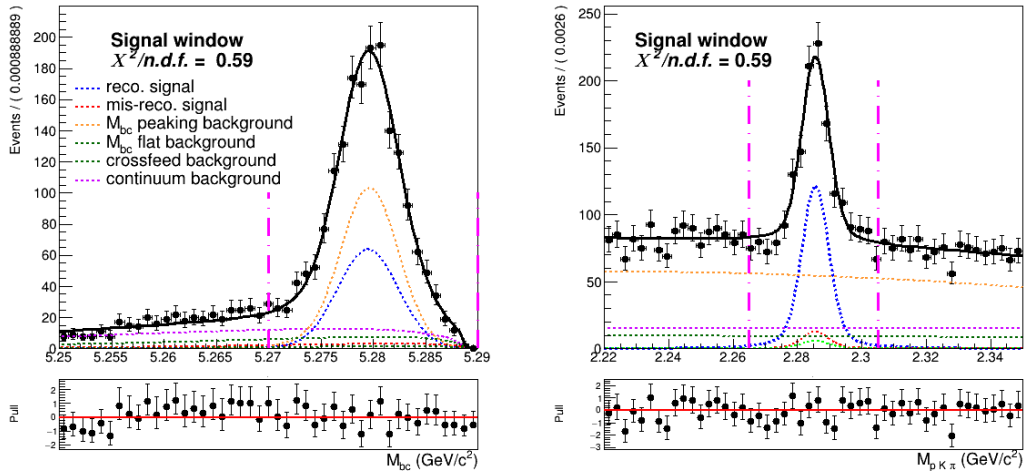


Figure (3.38) Projections of the two dimensional simultaneous fit on stream 0 Monte Carlo simulated data for neutral anticorrelated decays (in the signal window).

### 3.2.5 Fit residuals

Fig. 3.39 shows the residuals in each fit (stream by stream), calculated as the difference of reconstructed signal yield in the two dimensional fit from the expected value (in the fit of the total signal events). Since the signal events are the same in the two fits, the resulting yields are correlated. Therefore the uncertainties on the residuals are calculated (on a first approximation) as:

$$\sigma_{res} = \sqrt{(\sigma_{tot}^2 - \sigma_{sig}^2)} \quad (3.8)$$

Some of the results may seem not well distributed around 0.

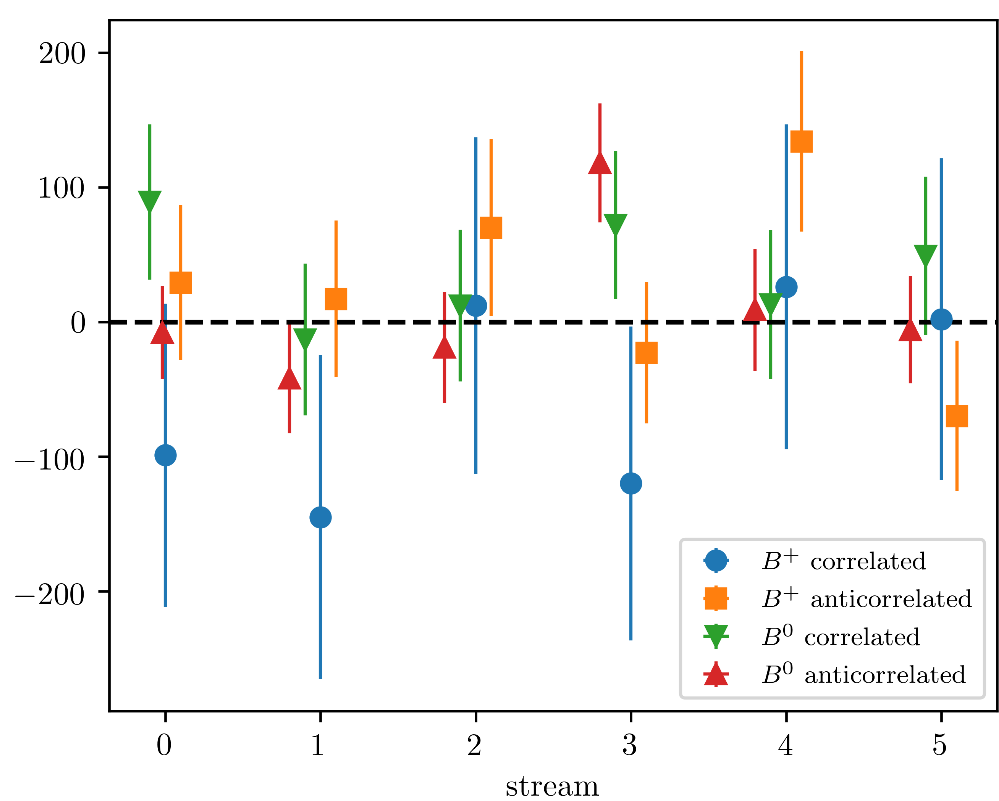


Figure (3.39) Residuals of the fitted signal yields resulting from the simultaneous 2D fit by stream and decay mode.

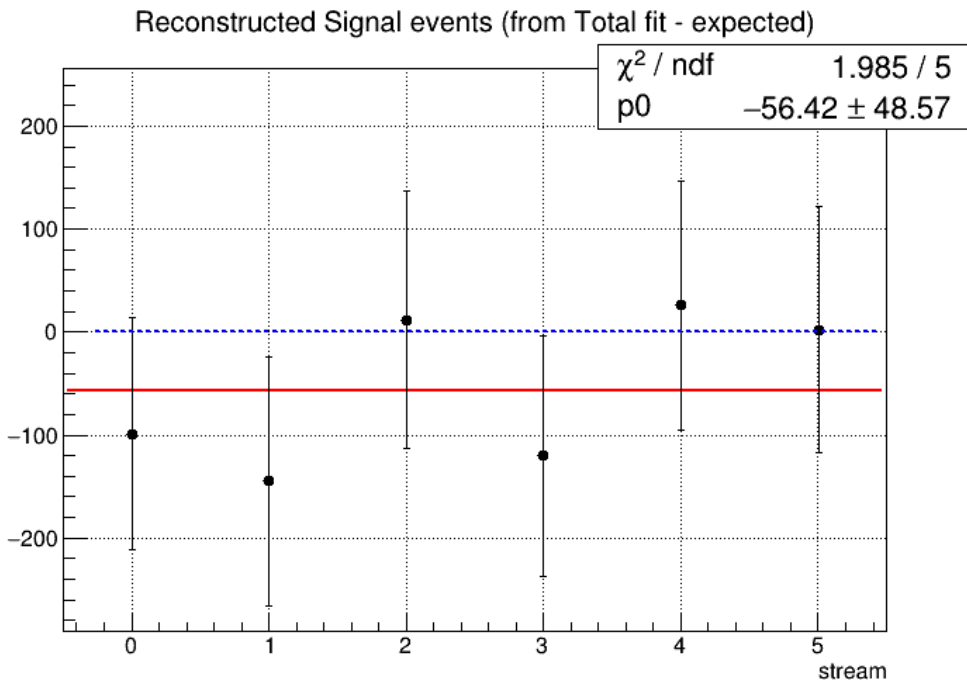


Figure (3.40) Residuals of the fitted signal yields of charged correlated decays.

### 359 3.2.6 toy Monte Carlo study

360 For the fit model also toy MC pseudo-experiments were performed in order to confirm  
 361 the behavior of the fit setup. With toy MC experiments the yields, errors and the pulls  
 362 of the fit are studied by generating our own pseudo-datasets, according to the MC (see  
 363 plots in  $3 \times 10^3$  pseudo-datasets are constructed, where each dataset was generated with  
 364 the expected amount of events, distributed according to the Poisson distribution. Then  
 365 the composition of each toy pseudo-experiment is fitted as if they were data, and the  
 366 pull-value distributions of the fit results are calculated. From the plots showing the pull  
 367 distributions of the fitted signal yields one can conclude that no bias is present.

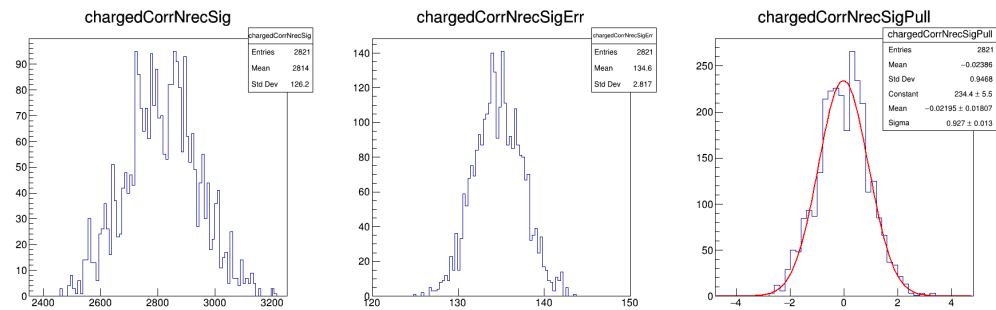


Figure (3.41) Plots showing distributions of the fitted signal yields, errors and the pull distribution of all pseudo-fits for the charged correlated decays.

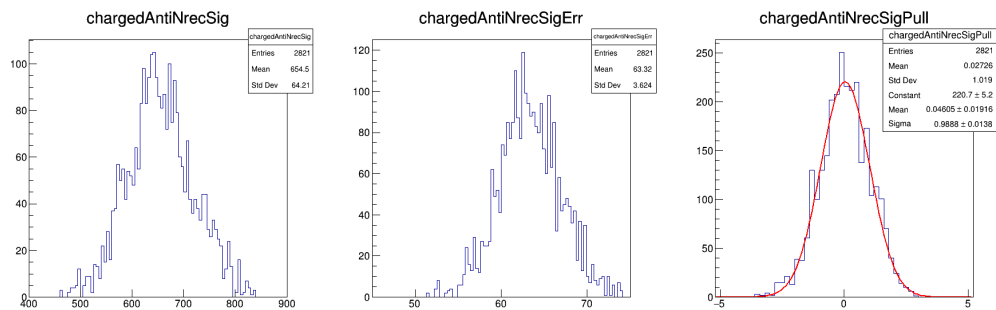


Figure (3.42) Plots showing distributions of the fitted signal yields, errors and the pull distribution of all pseudo-fits for the charged anticorrelated decays.

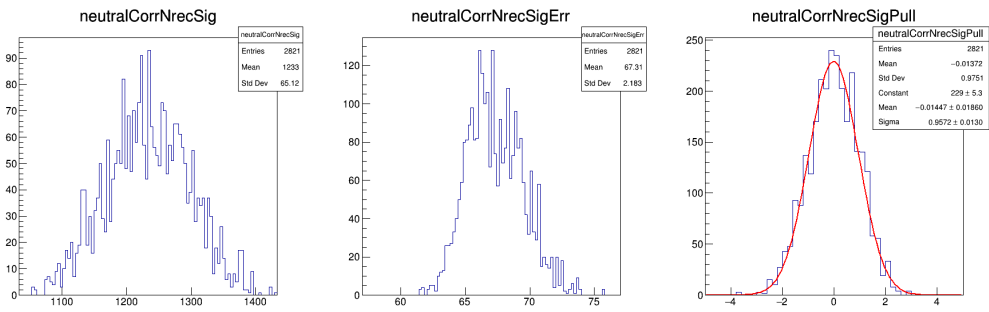


Figure (3.43) Plots showing distributions of the fitted signal yields, errors and the pull distribution of all pseudo-fits for the neutral correlated decays.

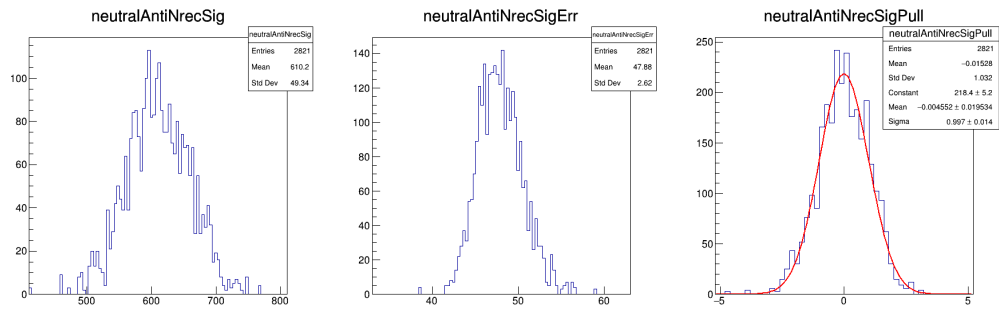


Figure (3.44) Plots showing distributions of the fitted signal yields, errors and the pull distribution of all pseudo-fits for the neutral anticorrelated decays.

368

# Chapter 4

369

## $B_{tag}$ fit

- 370 The normalization for the branching fractions is determined from the number of correctly  
371 tagged  $B$  mesons. This value is again determined by fitting the  $M_{bc}$  distribution of all  $B$   
372 meson candidates tagged by FEI regardless of the signal side  $B$  meson decay.  
373 The tagged  $B$  meson candidates are selected according to the selection criteria used for  
374 the  $M_{bc}$  variable already illustrated in subsections Secs. 2.4.1 to 2.4.4.

375

### 4.1 Probability Density Functions (PDFs) for the $B_{tag}$

376 The reconstructed events can be categorized as follows:

- 377     • correctly reconstructed  $B$  meson candidates: **reconstructed signal**  
378     • misreconstructed  $B$  meson candidates: **misreconstructed signal**  
379     •  $B^0$  mesons misreconstructed as  $B^+$  (and vice-versa): **crossfed background**  
380     • and **continuum background**

381

#### 4.1.1 Total Signal fits

382 As in the 2D fits the total signal is distinguished in **reconstructed** and **misreconstructed**  
383 **signal** depending on whether it's peaking or not in  $M_{bc}$ .  
384 Fig. 4.1 shows the fit on tagged charged  $B$  mesons corresponding to the normalization  
385 for the branching fractions of  $B^- \rightarrow \Lambda_c^+$  decays. The  $M_{bc}$  distribution of the tagged  $B$   
386 mesons is fitted with a combination of Crystal Ball and Gaussian as for the "peaking"  
387 component and the "flat" component is fitted with a Novosibirsk function. For the other  
388 decay channels instead an Argus function is used to describe the misreconstructed signal  
389 (see Figs. 4.2 to 4.4).

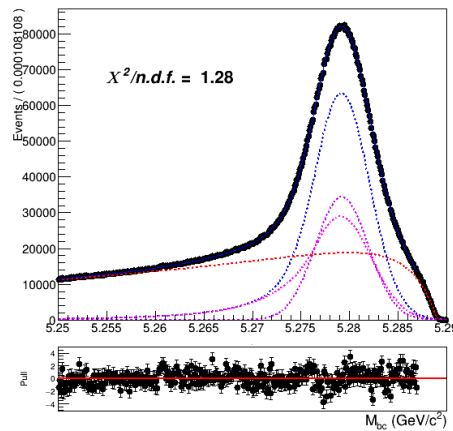


Figure (4.1) Fitted distribution of tagged charged  $B$  mesons in the charged correlated decays sample: reconstructed signal events are described by the blue dotted PDF, the misreconstructed with a Novosibirsk function (red dotted).

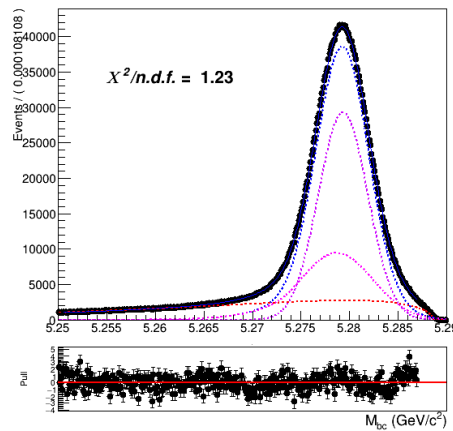


Figure (4.2) Fitted distribution of tagged charged  $B$  mesons in the charged anticorrelated decays sample.

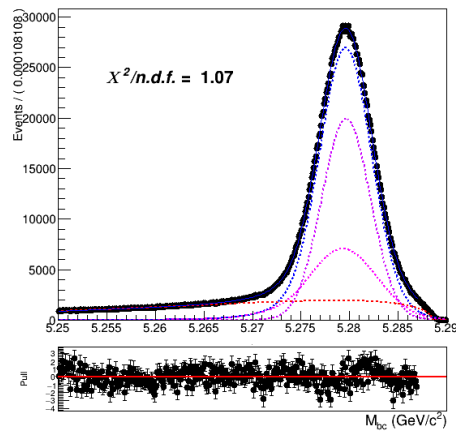


Figure (4.3) Fitted distribution of tagged neutral  $B$  mesons reconstructed in neutral correlated decays.

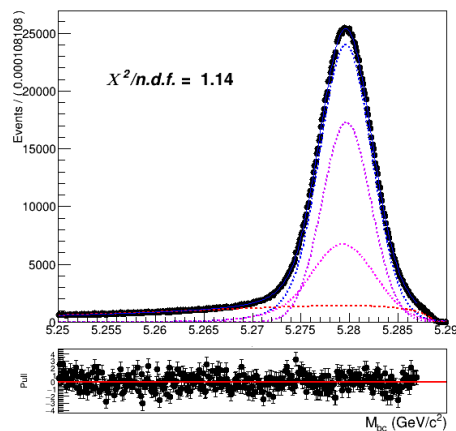


Figure (4.4) Fitted distribution of tagged charged  $B$  mesons reconstructed in neutral anticorrelated decays.

### 390 4.1.2 Crossfeed PDF

391 The crossfeed background is always fitted instead with a sum of a Novosibirsk and an  
 392 asymmetric Gaussian PDF.

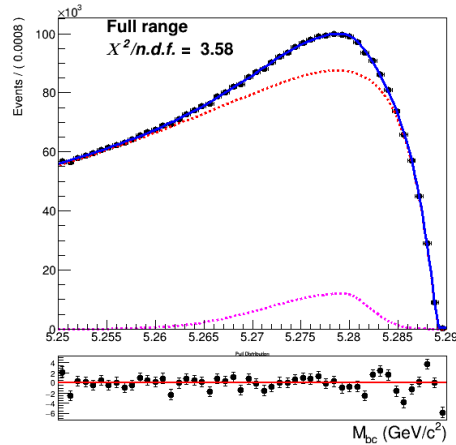


Figure (4.5) Crossfeed distribution of charged correlated decays fitted with a sum of Novosibirsk (red) and asymmetric Gaussian PDF (magenta)

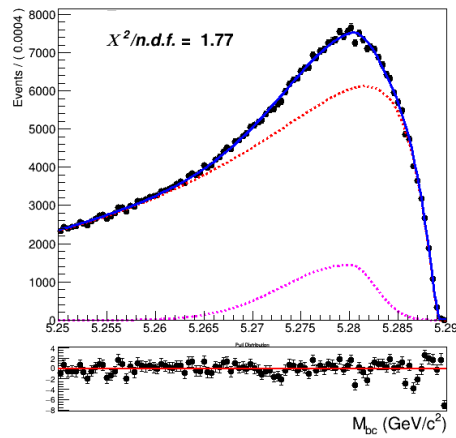


Figure (4.6) Crossfeed distribution of charged anticorrelated decays

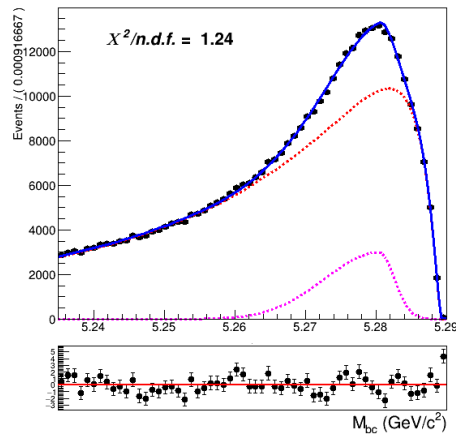


Figure (4.7) Crossfeed distribution of neutral correlated decays

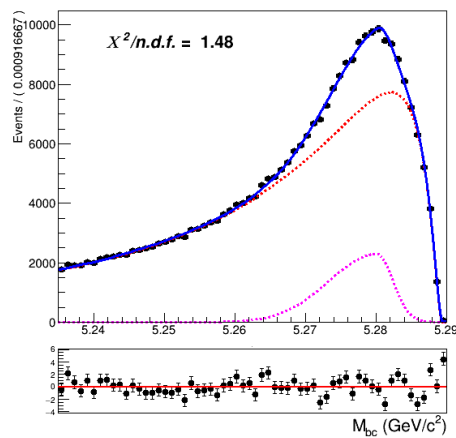


Figure (4.8) Crossfeed distribution of neutral anticorrelated decays

393 **4.1.3 Continuum PDF**

394 As for the continuum background, a similar procedure as the one described already for the  
 395 two dimensional fit was adopted:

- 396
- first the off-resonance sample is scaled accordingly

397

  - the ratio between the scaled off-resonance and the on-resonance in MC is calculated  
 398 in each bin (see Fig.4.9a)

399

  - the bin-correction is applied on an independent stream and the scaled and bin-  
 400 corrected  $M_{bc}$  distribution is compared with the on-resonance distribution as shown  
 401 in Fig.4.9b

402 Being the statistics much larger than in the 2D sample, there's no need to remove the  
 403 continuum suppression cut on the off-resonance sample.

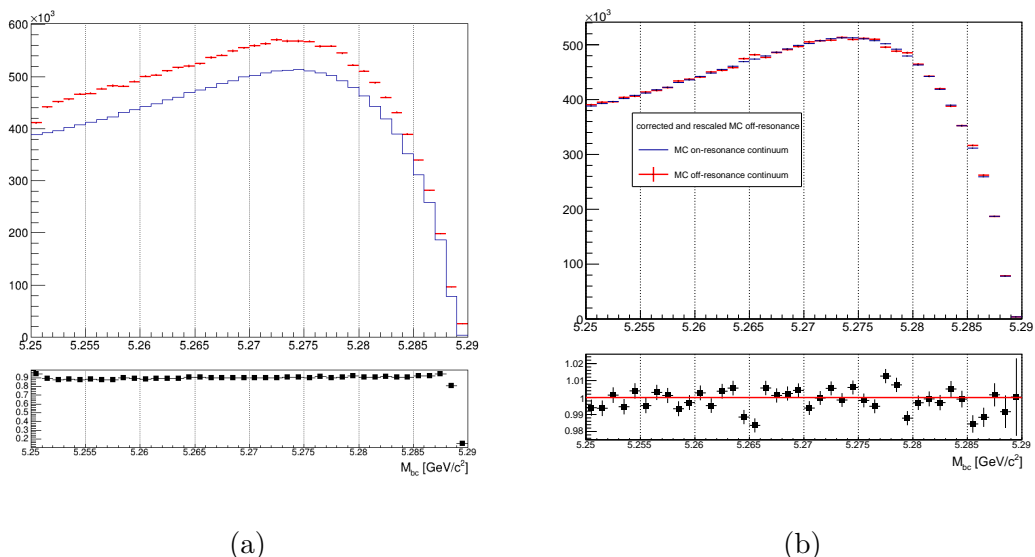


Figure (4.9) On the left:  $M_{bc}$  distributions of the MC off-resonance sample and the MC continuum sample with applied continuum suppression. On the right:  $M_{bc}$  distributions of the corrected scaled MC off-resonance and on-resonance MC continuum.

## 4.2 $B_{tag}$ fit

An independent Monte Carlo stream was used to test the total fit model on tagged  $B$  meson candidates. As in the 2D fit, the parameter for the width,  $\sigma_{CB}$ , of the Crystal Ball is floated. The ratio between expected crossfeed background events and misreconstructed signal events is fixed from the MC. The misreconstructed signal PDF is also not fully constrained: the parameter describing the tail is free. To avoid introducing significant systematic uncertainties in the fit deriving from the  $M_{bc}$  endpoint region, where one has a smearing effect due to variations of the beam energy at the MeV level, the range for the fit is restricted to values between 5.250 and 5.287  $\text{GeV}/c^2$ .

### 4.2.1 Fit results for $B^- \rightarrow \Lambda_c^+ \text{ decays}$

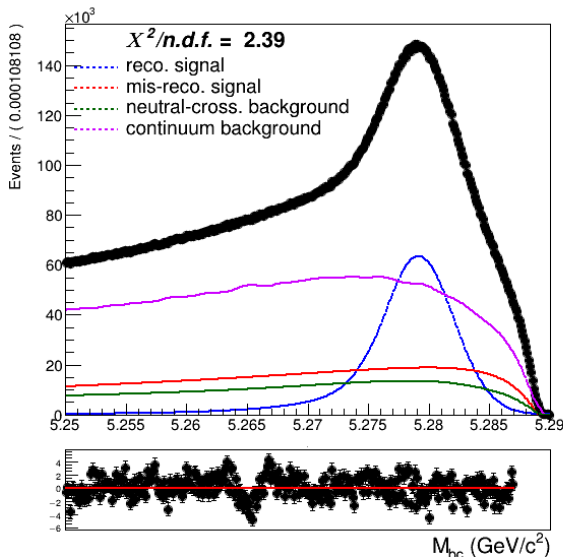


Figure (4.10) Total fit of tagged  $B$  mesons on Monte Carlo simulated data.

Yields for the reconstructed and misreconstructed signal are obtained from the fit:

	Fit results	expected
NrecSig	$4.7787 \cdot 10^6 \pm 6748$	$4.7571 \cdot 10^6 \pm 3214$
NmisSig	$5.3987 \cdot 10^6 \pm 5617$	$5.4035 \cdot 10^6 \pm 3376$

The normalization for the branching fraction is given by the NrecSig yields. The yields obtained in the fit differ by  $\sim 3.2\sigma$  from the expected ones (obtained from a fit to the Total Signal events only). This discrepancy will impact the final measurement.

420 To check the stability of the fit model a toy MC study was performed with  $3 \times 10^3$   
 421 pseudo-datasets. No evidence for possible biases in the reconstructed signal yields was  
 422 found (see Fig. 4.11).

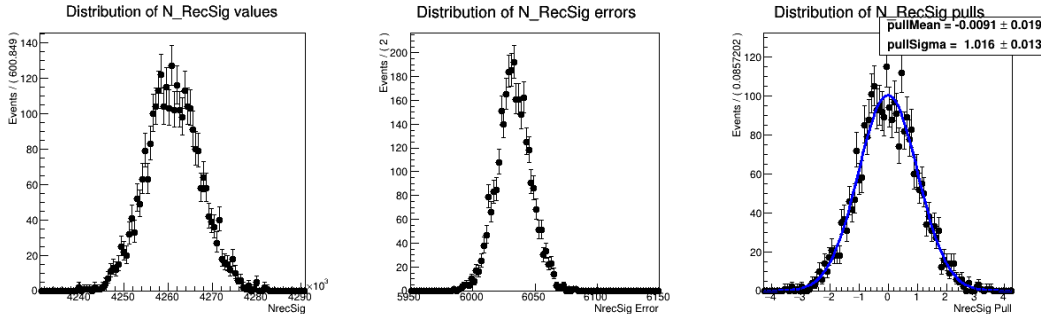


Figure (4.11) Plots showing distributions of the fitted signal yields, errors and the pull distribution of all pseudo-fits. (see Appendix ?? for the other free parameters' results)

#### 423 4.2.2 Fit results for $B^- \rightarrow \bar{\Lambda}_c^-$ decays

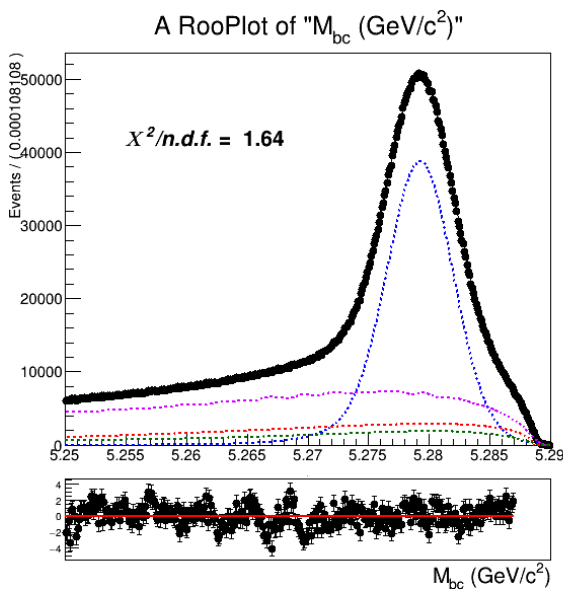


Figure (4.12) Total fit of tagged  $B$  mesons on Monte Carlo simulated data.

424

NrecSig	$2.50831 \cdot 10^6 \pm 11866$
NmisSig	$7.37010 \cdot 10^5 \pm 7472$

425 The Total Signal (the sum NrecSig+NmisSig) is  $3292168 \pm 2423$  (to be compared with  
 426 3299629 from the Monte Carlo), which means a  $\sim 3\sigma$  underestimation. As in the case of  
 427 charged flavor-correlated decays, this can produce some systematic effect which needs to  
 428 be taken into account.

429 But when performing a toy Monte Carlo study<sup>1</sup> the result show no bias on the  
 430 reconstructed signal yields (see Fig. 4.13)

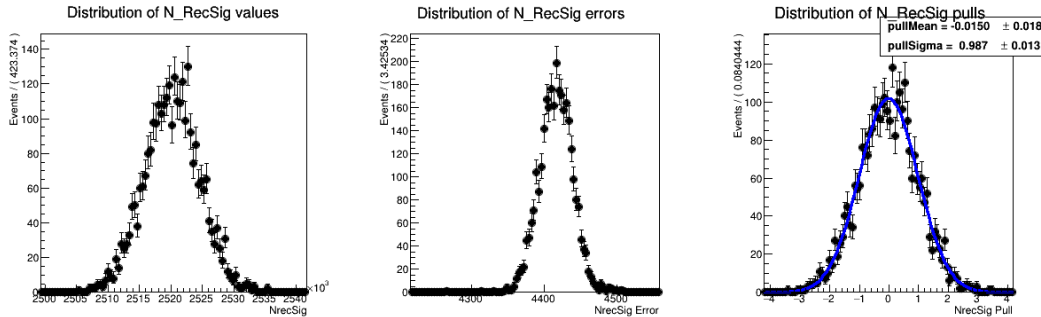


Figure (4.13) Plots showing distributions of the fitted signal yields, errors and the pull distribution of all pseudo-fits.

#### 431 4.2.3 Fit results for $\bar{B}^0 \rightarrow \Lambda_c^+$ decays

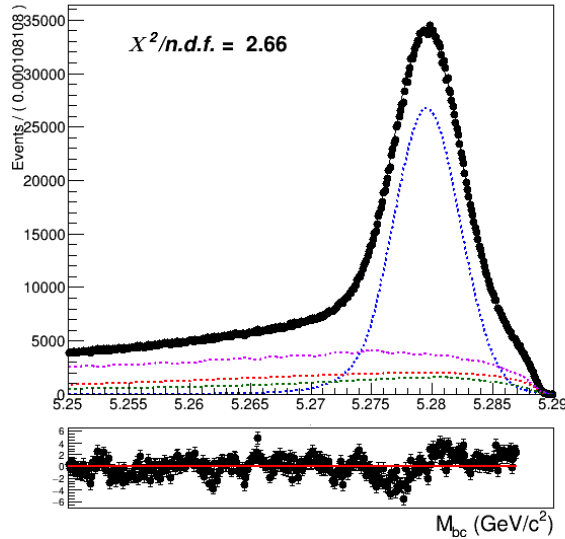


Figure (4.14) Total fit of tagged  $B$  mesons on Monte Carlo simulated data.

<sup>1</sup>as usual performed with  $3 \times 10^3$  pseudo-datasets

432 Reconstructed and misreconstructed signal yields obtained from the fit:

433

NrecSig	$1.7215 \cdot 10^6 \pm 3421$
NmisSig	$5.5950 \cdot 10^5 \pm 2215$

435 The Total Signal (the sum NrecSig+NmisSig) is  $2281033 \pm 1947$  (to be compared with  
436 2286964 from the Monte Carlo). Also in this case there's a  $\sim 3\sigma$  underestimation.

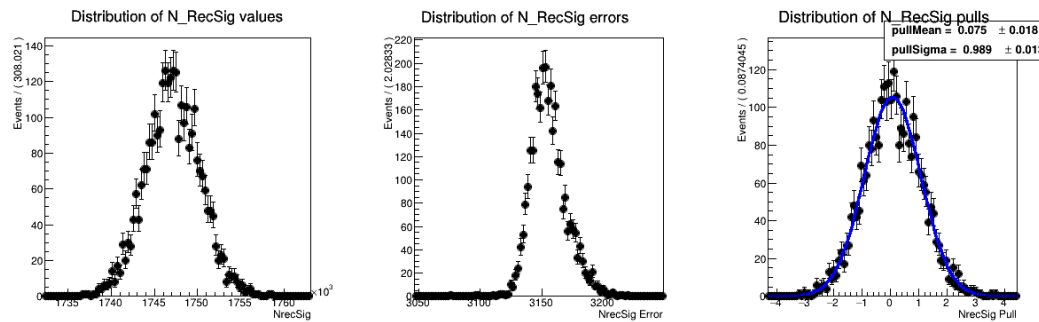


Figure (4.15) Plots showing distributions of the fitted signal yields, errors and the pull distribution of all pseudo-fits.

#### 437 4.2.4 Fit results for $B^0 \rightarrow \bar{\Lambda}_c^+$ decays

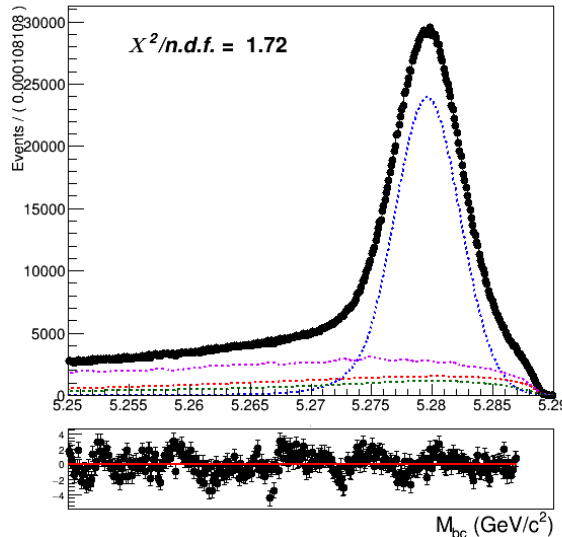


Figure (4.16) Total fit of tagged  $B$  mesons on Monte Carlo simulated data.

438 Reconstructed and misreconstructed signal yields obtained from the fit:

439

NrecSig	$1.5302 \cdot 10^6 \pm 3269$
NmisSig	$3.8332 \cdot 10^5 \pm 2072$

441 The Total Signal (the sum NrecSig+NmisSig) is  $1913476 \pm 1812$  (to be compared with  
442 1920156 from the Monte Carlo). Also in this case there is an underestimation of about a  
443  $\sim 3.7\sigma$ .

444 The toy MC study result for the signal yields is shown in Fig. 4.17. Also in this case  
445 no hints of bias are visible.

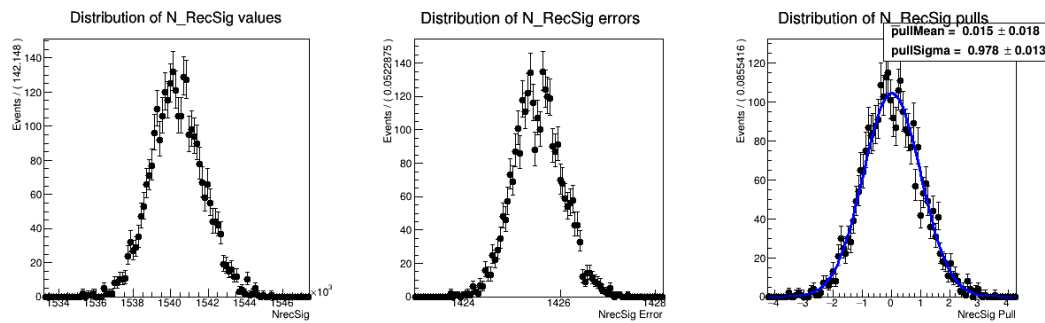


Figure (4.17) Plots showing distributions of the fitted signal yields, errors and the pull distribution of all pseudo-fits.

# 446 Chapter 5

## 447 Efficiencies

448 Here a decision was made not to rely on the estimated number of  $B$  meson pair, as it is  
449 usually done, and the absolute FEI efficiency, since the latter shows large discrepancy  
450 between MC and data (see i.e. the results reported in the PhD Thesis by M. Gelb [4] and  
451 also by J. Schwab [5] ) and also it depends strongly on the signal-side (i.e.  $\epsilon_{FEI}^+ \neq \epsilon_{FEI,sig}^+$ ).  
452 Instead, to limit the systematics, the branching ratio normalization is obtained using the  
453 fitted tagged  $B$  mesons and the ratio  $\epsilon_{FEI,sig}^+/\epsilon_{FEI}^+$  measured on MC, which one can expect  
454 to be better described by the MC than the absolute FEI efficiency.

### 455 5.1 FEI Efficiencies

456 One needs to distinguish two different FEI efficiencies as already anticipated.

457

458 The generic FEI efficiency  $\epsilon_{FEI} = \frac{n^{\circ} \text{oftagged}B}{\text{total}n^{\circ}\text{ofevents}}$  is the generic efficiency to tag correctly  
459 a  $B^+B^-$  or  $B^0\bar{B}^0$  event, i.e.: the hadronic decay-chain of the tag-side  $B$  meson is correctly  
460 reconstructed, independently from signal-side. The denominator is given by all  $B\bar{B}$  events  
461 present in the considered sample. The generic FEI efficiency is the one that affects the  
462 normalization in the branching ratio calculation.

463

464 The FEI efficiency that affects the numerator of the branching ratio is called signalside-  
465 dependent efficiency  $\epsilon_{FEI,sig}$ . In the case one is trying to reconstruct  $B^- \rightarrow \Lambda_c^+$  decays,  
466 then this efficiency is determined as the following ratio:  $\epsilon_{FEI,sig}^+ = \frac{n^{\circ} \text{oftagged}B^{+/-} \text{of } B^- \rightarrow \Lambda_c^+}{\text{total}n^{\circ} \text{of } B^- \rightarrow \Lambda_c^+ \text{ events}}$

#### 467 5.1.1 Generic FEI efficiency

468 The number of correctly tagged  $B$  mesons is determined from the yields of reconstructed  
469 signal events obtained from a fit of the  $B_{tag}$  distributions shown already in Sec. 4.1.1. As  
470 an example Fig. 5.1 shows the same distributions shown in Fig. 4.1 where all shaping  
471 parameters have been fixed and only the the normalisations of **reconstructed** and

472 misreconstructed signal were floated.

473

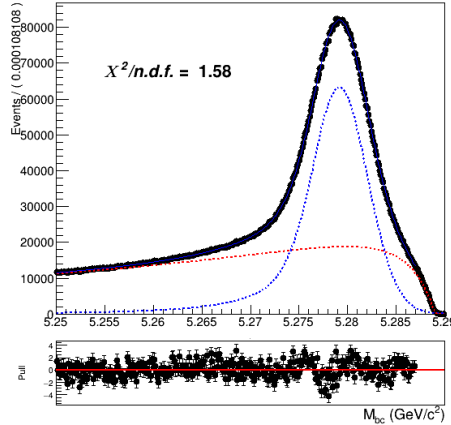


Figure (5.1) Fitted distribution of tagged charged B mesons in the charged correlated decays sample.

#### 474 5.1.2 Signalside-dependent FEI efficiency

475 The FEI tag-side efficiency for signal events is calculated upon 10 streams of on-resonance  
476 Monte Carlo streams of simulated data in order to minimize statistical uncertainties. As  
477 an example Fig. 5.2 shows the fit performed on the tagged  $B$  mesons having in the ROE a  
478 companion decaying  $B^- \rightarrow \Lambda_c^+$  (charged correlated decays). Dividing the yields obtained  
479 by the fit by the total number of  $B^- \rightarrow \Lambda_c^+$  events present in the 10 streams it is possible  
480 to determine the FEI tag-side efficiency for signal events.

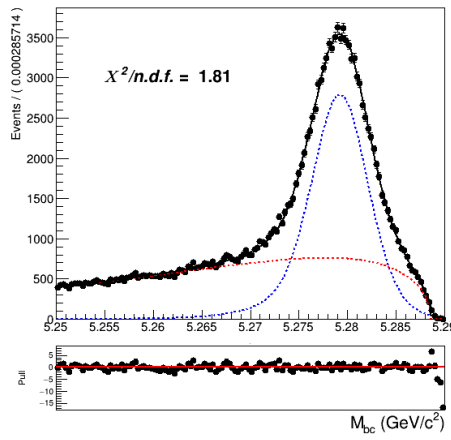


Figure (5.2) Fit of tagged  $B$  mesons in the "signal events" sample

481 **5.2  $\Lambda_c$  efficiency**

482 The efficiency of reconstructing the  $\Lambda_c$  baryon after correctly tagging the charged  $B$   
 483 meson, can be estimated from Monte Carlo simulated data. All available 10 streams of  
 484 on-resonance Monte Carlo streams of simulated data were used to minimize statistical  
 485 uncertainties. The efficiency is evaluated as follows from the fraction:

$$\frac{N_{recSig}(B_{tag}, \Lambda_c)}{N_{recSig}(B_{tag}^{sig})} \quad (5.1)$$

486 where  $N_{recSig}(B_{tag}, \Lambda_c)$ ) are the yields of reconstructed signal from a two dimensional fit of  
 487 corresponding inclusive decay. and  $N_{recSig}(B_{tag}^{sig})$  are the yields of correctly reconstructed  
 488 signal from the same fit of tagged  $B$  mesons used to calculate the Signalside-dependent  
 489 FEI efficiency.

490 **5.2.1  $B^- \rightarrow \Lambda_c^+$  decays**

491  $\epsilon_{FEI,sig}^+ = 0.636 \pm 0.003\%$  (calculated with 10 streams)

492  $\epsilon_{FEI}^+ = 0.6379 \pm 0.0004\% \frac{\epsilon_{FEI,sig}^+}{\epsilon_{FEI}^+} = 0.997 \pm 0.005$

493  $\epsilon_{\Lambda_c} = 37.78 \pm 0.45\%$

494 **5.2.2  $B^- \rightarrow \bar{\Lambda}_c^-$  decays**

495  $\epsilon_{FEI,sig}^+ = 0.334 \pm 0.003\%$  (calculated with 10 streams)

496  $\epsilon_{FEI}^+ = 0.3461 \pm 0.0002\%$  FEI calculation includes mixed events,  $\epsilon_{\Lambda_c}$  is calculated without

497 them  $\frac{\epsilon_{FEI,sig}^+}{\epsilon_{FEI}^+} = 0.965 \pm 0.009$

498  $\epsilon_{\Lambda_c} = 42.39 \pm 0.66\%$

499 **5.2.3  $\bar{B}^0 \rightarrow \Lambda_c^+$  decays**

500  $\epsilon_{FEI,sig}^+ = 0.247 \pm 0.002\%$  (calculated with 10 streams unmixed)

501  $\epsilon_{FEI}^+ = 0.236 \pm 0.0002\%$  (1 unmixed stream)

502  $\frac{\epsilon_{FEI,sig}^+}{\epsilon_{FEI}^+} = 1.056 \pm 0.010$

503  $\epsilon_{\Lambda_c} = 39.59 \pm 0.49\%$  (using unmixed events)

504 **5.2.4  $\bar{B}^0 \rightarrow \bar{\Lambda}_c^-$  decays**

505  $\frac{\epsilon_{FEI,sig}^+}{\epsilon_{FEI}^+} = 1.005 \pm 0.014$

506  $\epsilon_{\Lambda_c} = 41.49 \pm 1.13\%$

# 507 Chapter 6

## 508 Branching ratio

509 To measure the inclusive branching fractions

$$Br(B^{+/-} \rightarrow \Lambda_c^+ X) = \frac{N_{tag,\Lambda_c} \cdot \epsilon_{FEI}^+}{N_{tag} \cdot Br(\Lambda_c^+ \rightarrow pK^-\pi^+) \epsilon_{\Lambda_c} \epsilon_{FEI,sig}^+} \quad (6.1)$$

510

$$Br(B^0 \rightarrow \Lambda_c^{+/-} X) = \frac{N_{tag,\Lambda_c} \cdot \epsilon_{FEI}^0}{N_{tag} \cdot Br(\Lambda_c^+ \rightarrow pK^-\pi^+) \epsilon_{\Lambda_c} \epsilon_{FEI,sig}^0} \quad (6.2)$$

511

512 the following quantities need to be known:

- 513 •  $N_{tag,\Lambda_c}$  is the reconstructed signal yield obtained from a two dimensional fit of  $M_{bc}$   
514 and  $M(pK\pi)$  in the final sample.
- 515 •  $N_{tag}$  is the reconstructed signal yield obtained from the  $M_{bc}$  fit of all the tagged  $B$   
516 mesons in the final sample.
- 517 •  $\epsilon_{\Lambda_c}$  is the  $\Lambda_c$  reconstruction efficiency.
- 518 •  $\epsilon_{FEI}^+$  ( $\epsilon_{FEI}^0$ ) represent the hadronic tag-side efficiency for generic  $B^+B^-$  ( $B^0\bar{B}^0$ )  
519 events.
- 520 •  $\epsilon_{FEI,sig}^+$  ( $\epsilon_{FEI,sig}^0$ ) represents the hadronic tag-side efficiency for  $B^+B^-$  ( $B^0\bar{B}^0$ ) events  
521 where the tagged  $B$  meson decays hadronically and the accompanying meson decays  
522 inclusively into the studied signal channel.
- 523 •  $Br(\Lambda_c^+ \rightarrow pK^-\pi^+)$ : the branching fraction of the decay mode used to reconstruct  
524 the  $\Lambda_c$  baryon.

	total fit	signal fit	BELLE MC VALUE
stream 0	(2.84 ± 0.13)%	(2.96 ± 0.07)%	(2.91 ± 0.03)%
stream 1	(2.82 ± 0.14)%	(2.99 ± 0.07)%	(2.91 ± 0.03)%
stream 2	(2.97 ± 0.14)%	(2.97 ± 0.07)%	(2.90 ± 0.03)%
stream 3	(2.76 ± 0.14)%	(2.90 ± 0.07)%	(2.91 ± 0.03)%
stream 4	(3.06 ± 0.14)%	(3.05 ± 0.07)%	(2.90 ± 0.03)%
stream 5	(2.83 ± 0.14)%	(2.84 ± 0.07)%	(2.92 ± 0.03)%
average	(2.88 ± 0.06)%	(2.95 ± 0.03)%	(2.91 ± 0.01)%

Table (6.1) charged corr

	total fit	signal fit	BELLE MC VALUE
stream 0	(1.24 ± 0.11)%	(1.19 ± 0.05)%	(1.217 ± 0.002)%
stream 1	(1.24 ± 0.11)%	(1.21 ± 0.05)%	(1.218 ± 0.002)%
stream 2	(1.35 ± 0.12)%	(1.23 ± 0.05)%	(1.218 ± 0.002)%
stream 3	(1.16 ± 0.10)%	(0.20 ± 0.05)%	(1.215 ± 0.002)%
stream 4	(1.44 ± 0.13)%	(1.21 ± 0.05)%	(1.218 ± 0.002)%
stream 5	(1.04 ± 0.11)%	(1.15 ± 0.05)%	(1.217 ± 0.002)%
average	(1.25 ± 0.05)%	(1.20 ± 0.02)%	(1.217 ± 0.001)%

Table (6.2) charged anticorr

## 525 6.1 Systematics

### 526 6.1.1 Continuum background

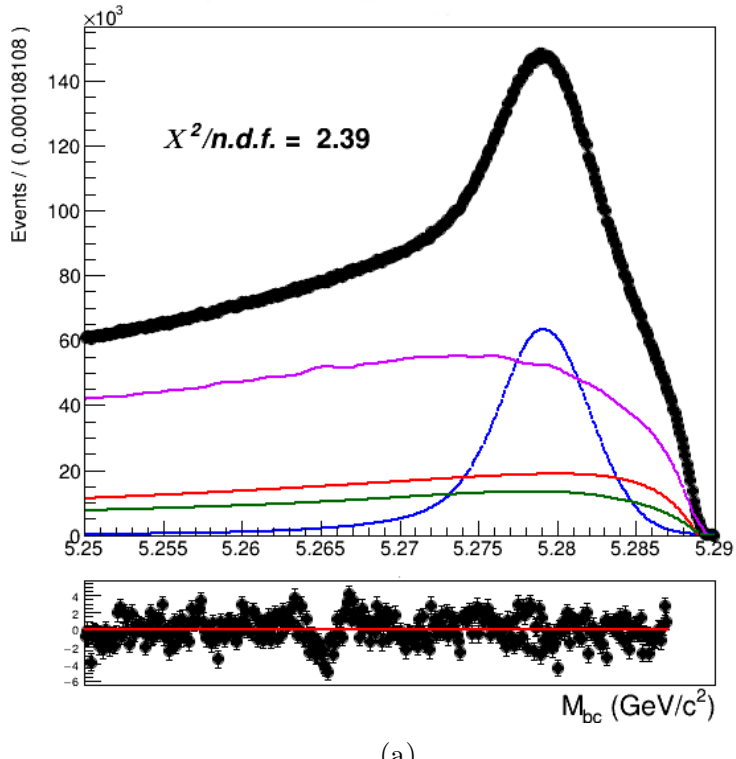
527 2 sources of systematics:

- 528
- difference in the shapes

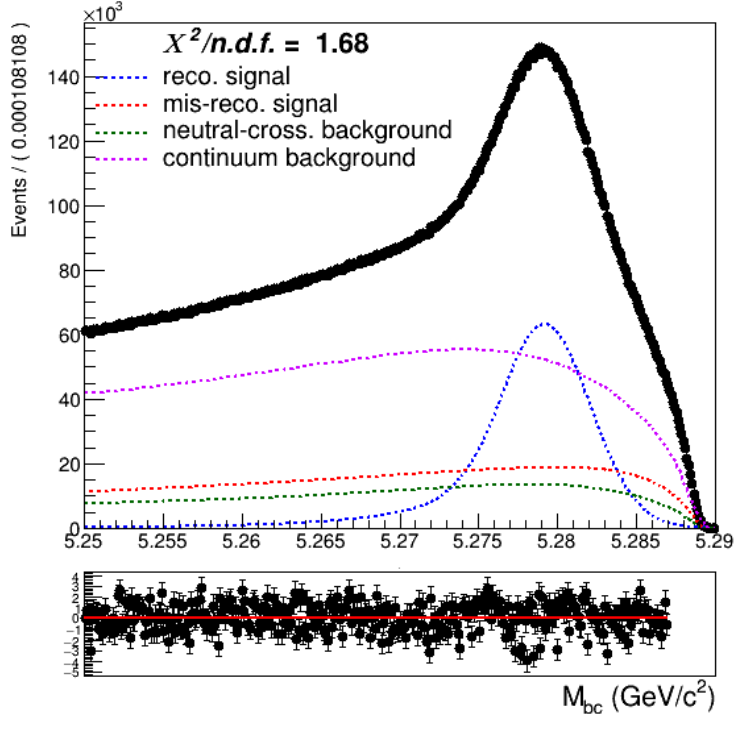
529

  - different impact of the Continuum Suppression cut

530 To estimate the first type of uncertainty two-dimensional fits with varied parameters'  
 531 values by their uncertainties (a fit with +err and -err) were performed.  
 532 The rescaling procedure used to model the on-resonance continuum distribution is far  
 533 from perfect, especially in the case of the  $B_{tag}$  fit. As one can see from Fig. 6.1a:  
 534



(a)



(b)

Figure (6.1) Above: Fitted  $M_{bc}$  of charged correlated decays with scaled off-resonance continuum distribution. Below: same  $M_{bc}$  distribution with the true continuum distribution.

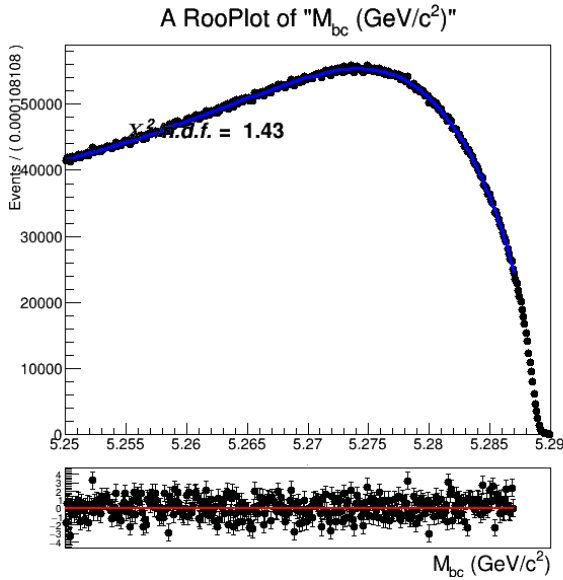


Figure (6.2)  $M_{bc}$  on-resonance MC distribution of charged correlated decays.

535     The bumps visible for  $M_{bc} < 5.27 \text{ GeV}/c^2$  in Fig. 6.1a are a consequence of the  
 536     imperfect scaling procedure used to model the continuum background. In fact, they  
 537     disappear completely (in Fig. 6.1b) when the same fit is performed using the pdf obtained  
 538     directly from the on-resonance distribution (Fig. 6.2) There is a significant impact on the  
 539     fit results, the values from the  $B_{tag}$  fit in the charged correlated channel are reported here  
 540     below:

	Fit with scaled continuum	Fit with true continuum
$N_{recSig}$ yields	$4.7787 \cdot 10^6 \pm 6.75 \cdot 10^3$	$4.7474 \cdot 10^6 \pm 8.01 \cdot 10^3$

Table (6.3) Signal yields obtained in  $B_{tag}$  fits shown in Fig. 6.1a and Fig. 6.1b.

541     The yields are to be compared with the values obtained when fitting the total signal  
 542     distribution shown in Fig. 4.1:  $N_{recSig} = 4.7571 \cdot 10^6 \pm 3.23 \cdot 10^3$ . The continuum modeling  
 543     alone is responsible for a discrepancy of about  $3.2\sigma$  on the yields. This discrepancy  
 544     and the impact on the branching fraction are accounted in the systematic uncertainties  
 545     derived from the continuum modeling. This source of systematics is responsible for  
 546     0.02 % uncertainty on the branching ratio. The other type of systematic uncertainty in  
 547     modeling the continuum is originated by the continuum suppression cut having a slightly  
 548     different efficiency on data (as a consequence of the shift in off-resonance MC and data  
 549     visible in the the *foxWolframR2* distribution in Fig. 3.19). As already discussed, it  
 550     originates a possible discrepancy of about 2.25% in continuum background events in the  
 551     two dimensional fit (and only 1.25% in the  $B_{tag}$  fit). The statistical uncertainty on this  
 552     fraction of events can also be taken into account as systematics. Being the number of

553 events in the off-resonance data sample without the continuum suppression applied is  
554 very small, the uncertainty in the mentioned fraction of events is negligible compared to  
555 the statistical uncertainty on the on-resonance continuum background events in MC: it  
556 would account for 0.002% on the BR value. Therefore, this second source of uncertainty is  
557 not taken into account. There would be also a third of systematic uncertainty given by  
558 potential difference in the on-/off-resonance correction between data and MC, but there's  
559 no way one can estimate it properly.

### 560 **6.1.2 Crossfeed ratio**

561 The ratio crossfeed/misreconstructed signal is kept fixed in the  $B_{tag}$  fit to the MC value.  
562 This choice was made according to the fact that the two categories of events have a similar  
563 origin: in both cases the  $B$  mesons were not correctly reconstructed, either because of  
564 missing or wrongly added particles (misreconstructed signal events) or, in the case of  
565 crossfeed events because the tagged  $B$  meson was not the required one ( $B^0$  meson instead  
566 of a  $B^{+/-}$  meson). The ratio between these two categories of events is therefore expected  
567 to be very similar in MC and data, though there's no guarantee that the efficiency to  
568 reconstruct them is the same in data and consequently the above mentioned ratios  
569 could differ on data. Unfortunately there's no direct way to have an estimate of the  
570 possible discrepancy for them.

571 In [4] (and previously in [5]) it was found that there's a substantial difference in terms of  
572 tagging efficiency for FEI applied on Monte Carlo and on Belle data, being the discrepancy  
573 around  $\sim 20\%$ . We can assume that the efficiency for the two categories of events on data  
574 will both differ of that value and the ratio of the events being the same MC value, but in  
575 absence of any other method to estimate the uncertainty on it one can consider a maximal  
576 discrepancy of 20% between Monte Carlo and data to study the impact on the yields<sup>1</sup>.

### 577 **6.1.3 Crossfeed $B_{tag}$ PDF**

578 Since also the shapes of the PDFs describing the crossfeed background in the  $B_{tag}$  fit are  
579 fully fixed to the ones determined with the limited Monte Carlo statistics, also their  
580 statistical uncertainties need to be taken into account as possible source of systematics. To  
581 estimate this source of uncertainty fits with varied parameters' values by their uncertainties  
582 (a fit with +err and -err) were performed.

### 583 **6.1.4 2DFit crossfeed normalization**

584 As discussed in the 2D simultaneous fit section, in each decay channel the normalization  
585 of crossfeed events is estimated using the fitted reconstructed signal events of the

---

<sup>1</sup>This method was also validated with the control decay sample and the originated uncertainty is well within the PDG reported ones.

586 corresponding crossfeeding channel in the as follows:

$$N_{cross} = N_{recSig}^{correlated} \left( \frac{\epsilon_{cross}}{\epsilon_{recSig}} \right)^{correlated} + N_{recSig}^{anticorrelated} \left( \frac{\epsilon_{cross}}{\epsilon_{recSig}} \right)^{anticorrelated} \quad (6.3)$$

587 where  $\epsilon_{recSig}$  and  $\epsilon_{cross}$  are respectively the efficiency to reconstruct correctly signal events  
 588 in the crossfeeding channel and the efficiency of reconstructing those events as crossfeed in  
 589 the channel of interest.

590 The uncertainties of those two efficiencies may cause an overestimation or underestimation  
 591 of the crossfeed in the channel of interest. To estimate the systematic uncertainty deriving  
 592 from it, the simultaneous fits have been performed modifying the ratio of the efficiencies  
 593 by the respective uncertainties maximising the shift, i.e. using  $\frac{\epsilon_{cross}+\sigma}{\epsilon_{recSig}-\sigma}$  and  $\frac{\epsilon_{cross}-\sigma}{\epsilon_{recSig}+\sigma}$

### 594 6.1.5 2DFit $M_{bc}$ peaking/flat PDFs

595 As discussed in ?? the shapes of the PDFs describing the generic background (peaking or  
 596 flat in  $M_{bc}$ ) are kept fixed in the two dimensional fit. This source of systematics is handled  
 597 in the same way as the crossfeed background in the  $B_{tag}$ : fits with varied parameters'  
 598 values by their uncertainties were performed (procedure is repeated for  $M_{bc}$  peaking and  
 599 flat background).

### 600 6.1.6 PID efficiency correction

601 The PID selection efficiency for the three charged particles in the signal decay needs to  
 602 be corrected on MC due to various differences, when comparing to data. The Belle PID  
 603 group has prepared a set of correction factors and tables of systematic uncertainties for  
 604 PID efficiencies for all charged particles. The proton identification efficiency was studied  
 605 in [6]. The inclusive  $\Lambda^0$  decay  $\Lambda^0 \rightarrow p\pi^-$  was used to examine the proton identification  
 606 efficiency difference between data and MC in *Belle*. The datasets for the SVD1 and SVD2  
 607 periods are treated separately, and the efficiency ratio dependence on proton charge,  
 608 momentum and polar angle is considered. The study is done for the proton ID cut values  
 609 0.6, 0.7, 0.8 and 0.9<sup>2</sup>. The binning on the momentum starts at 0.2 GeV. The proton ID  
 610 efficiency is defined as

611

$$612 \epsilon_{PID} = \frac{\text{number of } p\text{ tracks identified as } p}{\text{number of } p \text{ tracks}}$$

613

614 and the comparison between MC efficiency and data efficiency by a double ratio  
 615 defined as

616

$$617 R_p = \epsilon^{data}/\epsilon^{MC}$$

618

---

<sup>2</sup>Here, proton ID cut value  $X$  means  $\mathcal{L}_{p/K} > X$  and  $\mathcal{L}_{p/\pi} > X$

619 The average proton ID correction is estimated to be:  $R_p = 0.969 \pm 0.003$ .  
 620 The kaon identification efficiency was studied in detail in Belle Note 779 [7] ([http://belle.kek.jp/secured/belle\\_note/gn779/bn779.ps.gz](http://belle.kek.jp/secured/belle_note/gn779/bn779.ps.gz)). The decay  $D^{*+} \rightarrow D^0\pi^+$   
 621 followed by  $D^0 \rightarrow K^-\pi^+$ , was used to examine it. As for the proton identification efficiency  
 622 it considers the dependence on Kaon charge, momentum and polar angle and same ID cut  
 623 values<sup>3</sup>  
 624

### 625 6.1.7 $B^- \rightarrow \Lambda_c^+$ decays

626 Regarding the systematic uncertainties deriving from the continuum modeling in the  
 627 two-dimensional fit are estimated as already described in ?? one obtains an absolute value  
 628 of 0.04% on the branching fraction.  
 629 Instead the imperfect modeling of the continuum in the  $B_{tag}$  fit is responsible for a 0.02 %  
 630 on the branching fraction in absolute value.  
 631 Continuum modeling uncertainties account for 0.05% total uncertainties on the branching  
 632 fraction in absolute value.

633 To estimate the systematics derived from the crossfeed/misreconstructed signal ratio,  
 634 in the  $B_{tag}$  fit the number of crossfeed events were varied artificially in order to have  $\pm 20\%$   
 635 different ratio, keeping the previously determined Monte Carlo ratio fixed.

	$-\sigma$	$+\sigma$	$\pm\bar{\sigma}$
offset	20010	9330	14670

Table (6.4) Offsets on the  $N_{recSig}$  signal yields obtained varying of  $\pm 20\%$  the ratio of crossfeed/misreconstructed events in the  $B_{tag}$  fit and mean deviations reported in the last column.

636 The offsets that a potential  $\pm 20\%$  different crossfeed/misreconstructed signal ratio  
 637 produce results in 0.01% systematic uncertainty on the branching fraction.  
 638 The systematic uncertainties deriving from the crossfeed background modeling in the  $B_{tag}$   
 639 fit is estimated following the same procedure described for continuum modeling systematics  
 640 in the two dimensional fit.  
 641 In the table below the signal yields' offsets are listed changing the parameters within their  
 642 uncertainties, and the mean offsets value used to calculate the expected uncertainty on the  
 643 BR value. The resulting absolute systematic uncertainty is about 0.01% on the BR value.

---

<sup>3</sup>Here, Kaon ID cut value  $X$  means  $\mathcal{L}_{K/\pi} > X$ , so for values below  $X$  the tracks are identified as pions

	$-\sigma$	$+\sigma$	$\pm\bar{\sigma}$
offset	14810	17280	16045

Table (6.5) Offsets on the  $N_{recSig}$  signal yields obtained varying the parameters of crossfeed background PDFs within their uncertainties in the  $B_{tag}$  fit and mean deviations reported in the last column.

source	relative (%)	absolute (%)
Continuum modeling	1.77	0.05
$B_{tag}$ fit Crossfeed fraction	0.35	0.01
$B_{tag}$ fit Crossfeed PDF shape	0.35	0.01
2DFit crossfeed normalization	0.70	0.02
$M_{bc}$ peaking PDF shape	0.35	0.01
$M_{bc}$ flat PDF shape	0.35	0.01
$\epsilon_{FEI,sig}^+/\epsilon_{FEI}^+$	0.35	0.01
$\epsilon_{\Lambda_c}$	1.41	0.04
PID	1.75	0.05
Tracking efficiency	0.35	0.01
Total	3.18	0.09

Table (6.6) Systematic uncertainties in the determination of the  $B^+ \rightarrow \bar{\Lambda}_c^- X$  branching fraction in %.

### <sup>644</sup> 6.1.8 $B^+ \rightarrow \Lambda_c^+$ decays

<sup>645</sup> Regarding the systematic uncertainties deriving from the continuum modeling in the  
<sup>646</sup> two-dimensional fit are estimated one obtains an absolute value of 0.02% on the branching  
<sup>647</sup> fraction.

<sup>648</sup>

# <sup>649</sup> Bibliography

- <sup>650</sup> [1] B. Aubert et al., BaBar, *Study of inclusive  $B^-$  and  $\bar{B}^0$  decays to flavor-tagged  $D$ ,  $D_s$*   
<sup>651</sup> *and  $\Lambda_c^+$* , Phys. Rev. D **75** (2007) 072002, [arXiv:hep-ex/0606026](https://arxiv.org/abs/hep-ex/0606026).
- <sup>652</sup> [2] I. Grach, I. Narodetskii, S. Simula, and K. Ter-Martirosyan, *Exclusive and inclusive*  
<sup>653</sup> *weak decays of the  $B$ -meson*, Nuclear Physics B **502** (1997) no. 1-2, 227–248.
- <sup>654</sup> [3] Y. Hsiao, S.-Y. Tsai, C.-C. Lih, and E. Rodrigues, *Testing the  $W$ -exchange mechanism*  
<sup>655</sup> *with two-body baryonic  $B$  decays*, Journal of High Energy Physics **2020** (apr, 2020) .  
<sup>656</sup> [https://doi.org/10.1007/JHEP04\(2020\)035](https://doi.org/10.1007/JHEP04(2020)035).
- <sup>657</sup> [4] M. Gelb, *Search for the Rare Decay  $B^+ \rightarrow \ell^+ \nu_\ell \gamma$  with the Full Event Interpretation at*  
<sup>658</sup> *the Belle Experiment*. PhD thesis, Karlsruhe Institute of Technology (KIT), 2018.
- <sup>659</sup> [5] J. Schwab, *Calibration of the Full Event Interpretation for the Belle and the Belle II*  
<sup>660</sup> *Experiment*, Master's thesis, Karlsruhe Institute of Technology (KIT), 2017.
- <sup>661</sup> [6] K.-J. Tien and M.-Z. Wang, *Proton identification efficiency study*, BELLE NOTE 1279.
- <sup>662</sup> [7] S. Nishida, *Study of Kaon and Pion Identification Using Inclusive  $D^*$  Sample*, BELLE  
<sup>663</sup> NOTE 779.